Single molecule analysis of CENP-A chromatin by high-speed atomic force microscopy

Daniël P Melters[1]*, Keir C Neuman[2]*, Reda S Bentahar[1], Tatini Rakshit[1,3], Yamini Dalal[1]*

[1]National Cancer Institute, Center for Cancer Research, Laboratory Receptor Biology and Gene Expression, Bethesda, United States; [2]National Heart, Lung, and Blood Institute, Laboratory of Single Molecule Biophysics, Bethesda, United States; [3]Department of Chemistry, Shiv Nadar University, Dadri, India

Abstract Chromatin accessibility is modulated in a variety of ways to create open and closed chromatin states, both of which are critical for eukaryotic gene regulation. At the single molecule level, how accessibility is regulated of the chromatin fiber composed of canonical or variant nucleosomes is a fundamental question in the field. Here, we developed a single-molecule tracking method where we could analyze thousands of canonical H3 and centromeric variant nucleosomes imaged by high-speed atomic force microscopy. This approach allowed us to investigate how changes in nucleosome dynamics in vitro inform us about transcriptional potential in vivo. By high-speed atomic force microscopy, we tracked chromatin dynamics in real time and determined the mean square displacement and diffusion constant for the variant centromeric CENP-A nucleosome. Furthermore, we found that an essential kinetochore protein CENP-C reduces the diffusion constant and mobility of centromeric nucleosomes along the chromatin fiber. We subsequently interrogated how CENP-C modulates CENP-A chromatin dynamics in vivo. Overexpressing CENP-C resulted in reduced centromeric transcription and impaired loading of new CENP-A molecules. From these data, we speculate that factors altering nucleosome mobility in vitro, also correspondingly alter transcription in vivo. Subsequently, we propose a model in which variant nucleosomes encode their own diffusion kinetics and mobility, and where binding partners can suppress or enhance nucleosome mobility.

*For correspondence:
daniel.melters@nih.gov (DPM);
neumankc@nhlbi.nih.gov (KCN);
dalaly@mail.nih.gov (YD)

Editor's evaluation

This is an interesting paper that describes the validation of high speed AFM as a tool for measuring the dynamics of individual nucleosomes in vitro. After validating the methodology the authors go on to apply the method to nucleosomes containing the centromere-specific histone variant CENP-A, and they show that addition of the CENP-A binding factor CENP-C radically alters the mobility of centromeric nucleosomes.

Introduction

Regulating physical access to DNA is central to both gene expression, genome topology, and genome integrity across eukaryotes. Decades of data strongly suggest that more physically accessible chromatin is also more transcriptionally permissive (*Klemm et al., 2019*; *Maeshima et al., 2019* landmark papers from *Weintraub and Groudine, 1976*; *Wu et al., 1979*). In contrast, compacted chromatin or heterochromatin has been correlated with transcriptional restriction (*Allshire and Madhani, 2018*; *Flamm et al., 1969*; *Janssen et al., 2018*; *Schultz, 1936*). These chromatin states are dynamic and

subject to tight regulation. Chromatin-binding proteins dictate many of these dynamics in part driven by the presence and deposition of specific post-translational modifications (PTMs) of nucleosomes (*Chung et al., 2023*; *Rothbart and Strahl, 2014*; *Taverna et al., 2007*; *Tolsma and Hansen, 2019*). For instance, HP1 binds to H3K9me2/3 nucleosomes (*Bannister et al., 2001*; *Nakayama et al., 2001*; *Lachner et al., 2001*; *Sanulli et al., 2019*), ultimately resulting in transcriptionally repressive chromatin (*Bannister et al., 2001*; *Escobar et al., 2021*; *Hwang et al., 2001*; *Nakayama et al., 2001*; *Lachner et al., 2001*). Interestingly, upon binding of HP1 to H3K9me3 nucleosomes, these nucleosomes' internal residues become more exposed to hydrogen/deuterium exchange (*Sanulli et al., 2019*). This seminal finding suggests that chromatin-binding proteins not only serve as a recruitment platform for other binding proteins but can rapidly alter the physical properties of individual nucleosomes. The logical extension of this concept is examining how altering innate physical properties of nucleosomes modulates the local chromatin state's structure and function.

To study how nucleosome dynamics is altered by chromatin binding factors, single molecule techniques have been developed, ranging from groundbreaking in vitro techniques such as optical and magnetic tweezers (*Bustamante et al., 2021*; *Chien and van Noort, 2009*; *Killian et al., 2018*; *Neuman and Nagy, 2008*) and in vivo single molecule tracking (*Iida et al., 2022*; *Izeddin et al., 2014*; *Mueller et al., 2013*; *Shen et al., 2017*; *van Staalduinen et al., 2023*; *Wang et al., 2021*). The former two techniques rely on precisely designed DNA sequences and constructs to guarantee precise measurements. By manipulating an optical trap or magnetic tweezer, tension and torsion forces can be exerted on the associated DNA molecule, which in turn alters the forces exerted on nucleosomes (*Bustamante et al., 2021*; *Chien and van Noort, 2009*; *Killian et al., 2018*; *Neuman and Nagy, 2008*). In contrast, single molecule tracking in cells is made possible by photostable fluorophores covalently bound to a target protein. These tagged proteins are introduced into cells at low concentration to allow the tracking of single molecules, with limited control where the tagged proteins will go (*Iida et al., 2022*; *Mueller et al., 2013*; *Shen et al., 2017*; *Wang et al., 2021*). Both systems are powerful and have distinct advantages, ranging from bp-precision of nucleosome sliding, folding-unfolding dynamics to determining residency time of transcription factors. However, a gap exists connecting these two technical approaches, namely assessing, and quantifying the dynamics of individual nucleosomes and correlating them with global chromatin dynamics. High-speed atomic force microscopy (HS-AFM) has the capability to span this gap. It is an in vitro based technique that permits real time tracking of single molecules in the context of interacting macromolecular complexes (e.g. myosin tracking on actin filaments, *Ando, 2018*; chromatin techniques reviewed in *Melters and Dalal, 2021*). By imaging nucleosome arrays in buffer over time, it is possible not just to track, but also quantify the motions of individual nucleosomes within an array.

In addition to PTMs, the chromatin landscape is also marked by the local enrichment of histone variants (*Buschbeck and Hake, 2017*; *Jamge et al., 2023*; *Martire and Banaszynski, 2020*; *Melters et al., 2015*), such as the centromere-specific H3 histone variant CENP-A/CENH3. CENP-A nucleosomes recruit several centromeric proteins (*Walstein et al., 2021*; *Mendiburo et al., 2011*; *Régnier et al., 2005*), including CENP-C. CENP-C in turn functions as the blueprint for the formation of the kinetochore (*Cheeseman et al., 2006*; *DeLuca and Musacchio, 2012*; *Hara et al., 2023*; *Walstein et al., 2021*; *Przewloka et al., 2007*; *Weir et al., 2016*; *Yatskevich et al., 2023*). Recently, we reported that the central domain of CENP-C (CENP-C^{CD}) induces loss of CENP-A nucleosomal elasticity in silico and in vitro (*Melters et al., 2019*). This finding correlates with decreased hydrogen/deuterium exchange of CENP-A nucleosomes when bound by CENP-C^{CD} (*Falk et al., 2016*; *Falk et al., 2015*; *Guo et al., 2017*). Interestingly, CENP-C knock-down resulted in downregulation of centromeric transcription (*Bury et al., 2020*), whereas CENP-C overexpression resulted in reduced RNA polymerase 2 (RNAP2) levels at the centromere and clustering of centromeric chromatin (*Melters et al., 2019*). We were curious about how CENP-A alone, and in combination with CENP-C mechanistically impacts centromeric chromatin fiber mobility. To address this question, we employed HS-AFM to track thousands of canonical or centromeric nucleosomes in arrays in real time. We report that HS-AFM imaging is free of tip-induced artifacts and CENP-A chromatin responds predictably to various control conditions. Next, we find that the essential kinetochore protein CENP-C, which is CENP-A chromatin's closest binding partner, directly impacts nucleosome mobility and, surprisingly, also chromatin fiber motion in vitro. These data represent a technological advance in imaging and analyzing chromatin dynamics by HS-AFM. We extended these findings in vivo using immunofluorescence imaging and biochemical

approaches, reporting that overexpressing CENP-C alters centromeric chromatin transcription and the ability to load new CENP-A molecules. Cumulatively, these data support the notion that local transcriptional competency depends on innate properties and local homeostasis of histone variants within the chromatin fiber in vivo.

Results

We are interested in understanding how nucleosomes 'behave' in biologically relevant conditions. Elegant single-molecule techniques have enabled us to understand details about the movement of transcription factors inside the nucleus (*Iida et al., 2022*; *Mueller et al., 2013*; *Shen et al., 2017*; *Wang et al., 2021*) and how torsion and pulling/pushing forces influence nucleosomes (*Bustamante et al., 2021*; *Chien and van Noort, 2009*; *Killian et al., 2018*; *Neuman and Nagy, 2008*). Although the behavior of a single trajectory might be stochastic, the statistical behavior from many trajectories may reveal additional physical properties, such as diffusion and folding-unfolding dynamics.

By directly observing topographic characteristics and dynamics of chromatin using HS-AFM, we were able to assess the motions of individual nucleosomes in real-time (*Figure 1*). This emerging single-molecule technique is powerful, and shares similarities with live cell imaging (*Ashwin et al., 2019*; *Specht et al., 2017*), magnetic tweezers, and optical tweezers (*Bustamante et al., 2021*; *Chien and van Noort, 2009*; *Killian et al., 2018*; *Neuman and Nagy, 2008*). Whereas, live cell imaging and single-molecule force spectroscopy methods rely on fluorophore-tags and tethering, HS-AFM can be done on both unmodified and modified protein all while requiring minimal sample preparation (*Ando, 2018*).

Recently, we showed by HS-AFM that, at a qualitative level, H3 nucleosomes are mobile and make intermittent contact with other H3 nucleosomes (*Melters and Dalal, 2021*). Here, we set out to quantify the dynamics of individual nucleosomes in the context of chromatin. This means that we observed and quantified global nucleosome movement on mica surface, which can be one-dimenstional motion of nucleosome sliding along DNA events and two-dimensional whole chromatin fiber movements (*Figure 1*). Nucleosomes that move away from the mica surface into the buffer solution could not be tracked. We predict that these global nucleosome motions reflect the complex dynamics nucleosomes display in the nucleus (*Ide et al., 2022*). To assay CENP-A chromatin, we reconstituted CENP-A nucleosomes on a~3.5 kbp plasmid containing four copies of α-satellite repeats or a~8.5 kbp plasmid containing three copies of the PCAT2 lncRNA gene. After verifying successful in vitro chromatin reconstitution (*Figure 1—figure supplement 1*, *Figure 1—figure supplement 1—source data 1 and 2*), we imaged CENP-A chromatin using the Cypher VRS system (see Materials and methods for details). Videos were obtained at one second per frame. When the AFM tip scans the mica surface, it first goes from the top to the bottom, followed by from the bottom to the top. To avoid discontinuous scanning of the same regions of the mica surface, we limited our analysis to every other frame, resulting in an effective scanning rate of two seconds per frame. Next, the videos were converted to TIFF sequences. Using MATLAB's single particle tracking MatlabTrack package, we obtained a total of 6052 individual nucleosome trajectories from 13 different samples (see Materials and methods for details). To obtain significant mean square displacement (MSD) values, individual trajectories needed to be of sufficient duration. Therefore, we selected individual trajectories that were at least 20 s, with a maximum of 120 s (10–60 points). In addition, we wanted to make sure that we were tracking the same nucleosomes, so we estimated the maximum single step size at twice the nucleosome width or 24 nm. Furthermore, we were also careful about potential nucleosomes sticking to the mica surface, which led us to reject trajectories with an average R-step size (the displacement between two successive images) smaller than 1 nm and a maximum R range smaller than 8 nm. Next, we corrected each video for drift (*Figure 1—figure supplement 2*). Finally, we analyzed 3835 trajectories to obtain the step angle, step size, mean square displacement (MSD), and diffusion constant of individual nucleosomes (*Figure 1*).

HS-AFM imaging is free of tip-induced artifacts

AFM is a topographical imaging technique that creates a sub-nanometer scale topological map of biological samples. A common concern is that the AFM tip may alter the sample during scanning, as the AFM tip moves in a zig-zag manner across the sample, potentially moving biological material
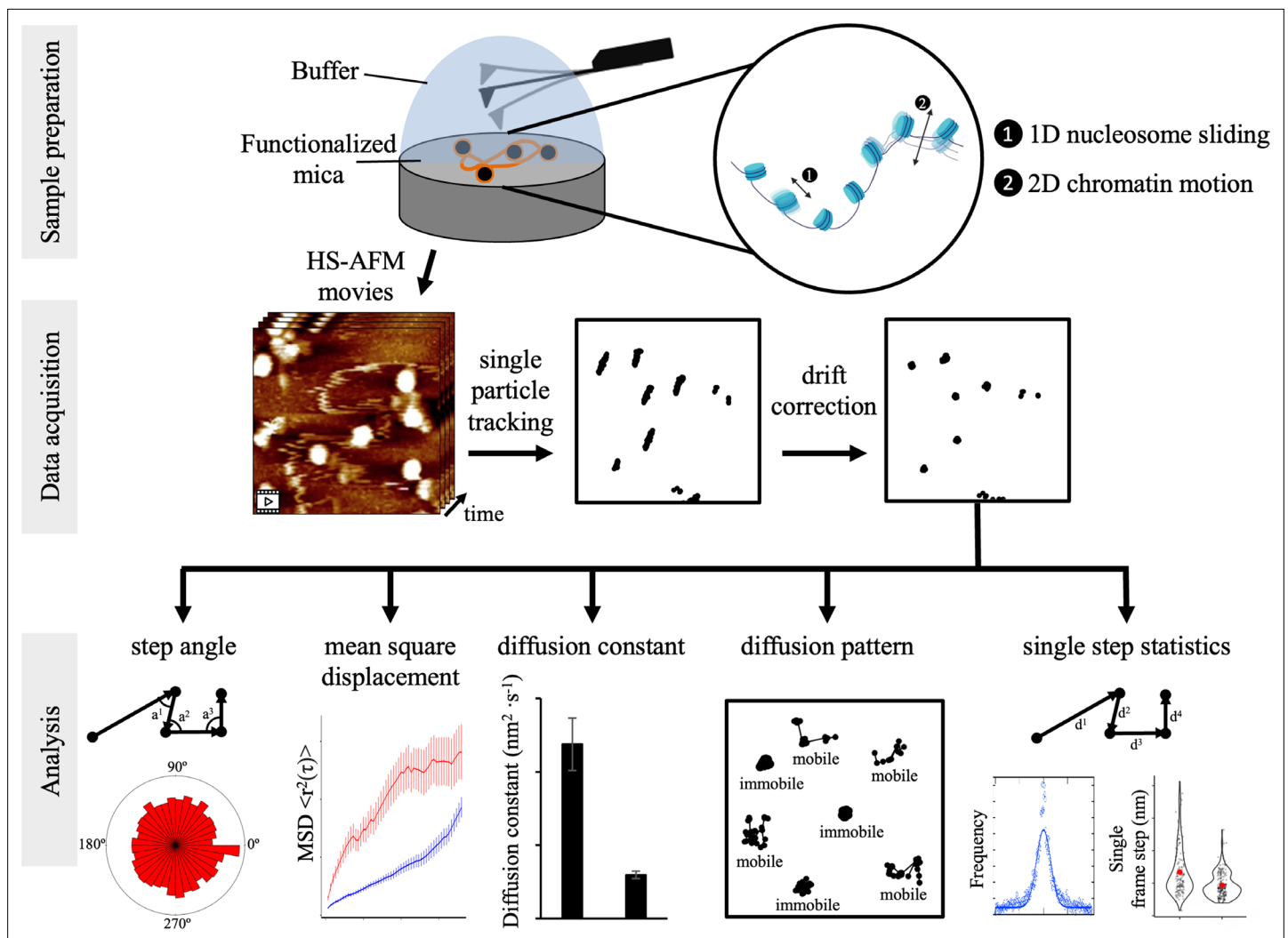
Figure 1. Schematic of experimental configurations for HS-AFM nucleosome measurements and analysis of extracted single particle trajectories Sample preparation: CENP-A nucleosomes were in vitro reconstituted and imaged by HS-AFM in fluid. By HS-AFM, we can track nucleosome motion, corresponding to both nucleosomes sliding along the DNA and chromatin fiber moving. Data acquisition: HS-AFM videos were obtained at a framerate of 0.5 Hz (2 s per frame) for a minimum of 20 s and up to 120 s. Using MATLAB, we extracted nucleosome trajectories, which were subsequently corrected for drift. Analysis: trajectories were analyzed to extract several mobility and diffusion-related parameters to determine both potential tip-scanning artifacts and to characterize nucleosome dynamics.

The online version of this article includes the following source data and figure supplement(s) for figure 1:

Figure supplement 1. Confirmation of *in vitro* reconstitution of CENP-A chromatin.

Figure supplement 1—source data 1. Complete gels for *Figure 1—figure supplement 1A* (12% SDS-PAGE) and 1 C (1% agarose gel).

Figure supplement 1—source data 2. Nucleosome statistics for each nucleosome for nucleosome diameter (nm), nucleosome height (nm), and nucleosome volume (nm^3).

Figure supplement 2. Drift correction of HS-AFM videos.

in its path. To determine whether there is indeed a tip effect, we performed several controls. We reasoned that if the AFM tip altered samples during scanning, it would create a distinctive signature in single particle trajectories. We imaged CENP-A chromatin under multiple conditions (*Figure 2— videos 1–6*). First, we assessed the angle between successive steps of the nucleosomes (*Figure 2A*). If there was tip-induced drift, there would be a bias in the distribution of angles. We did not observe a bias in the angle distributions (*Figure 2B*; *Figure 2—figure supplement 1A*, *Figure 2—source data 1*). Second, we looked at the diffusion constants over the x-axis alone or the y-axis alone (*Figure 2C*) in the absence or presence of 1-(3-aminopropyl) silane (APS). APS functionalizes the mica surface
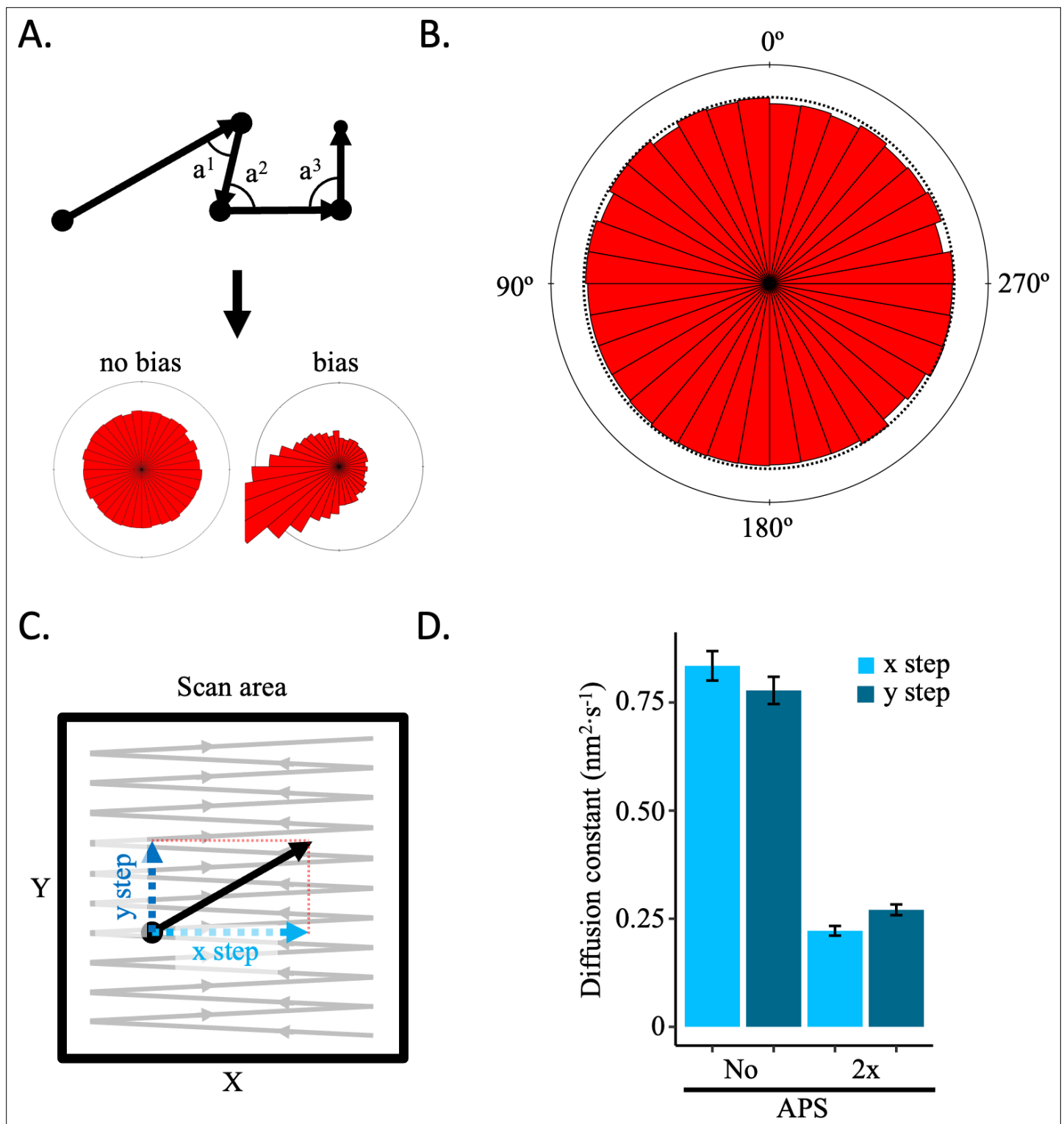
Figure 2. No AFM tip-motion effect was observed. If the AFM tip were to displace the sample during scanning, it should result in a motion bias in the direction of scanning that can be detected. (**A**) Schematic representation of how angle between successive steps within a trajectory is determined and representative angle distribution graphs for no bias or bias. (**B**) All angles for successive steps of all trajectories of five control conditions (low salt, high salt, no APS, 2 x APS, and Tween-20) show no sign of bias (*Figure 2—figure supplement 1A*). (**C**) Every step has an x and y coordinate. By obtaining the diffusion constant for each axis separately, motion bias between the x and y axis can be discerned, which is an indication of bias introduced by the AFM tip. (**D**) The diffusion constants for the x and y axis for CENP-A nucleosomes in low or high salt conditions show differences between imaging conditions, but not within each condition (*Figure 2—figure supplement 1B*). The error bars represent the standard error.

Figure 2 continued on next page

Figure 2 continued

The online version of this article includes the following video, source data, and figure supplement(s) for figure 2:

Source data 1. Trajectory statistics for all tracked nucleosomes.

Source data 2. Basic statistics for all tracked nucleosomes.

Figure supplement 1. No AFM tip-motion effect observed across control conditions.

Figure supplement 1—source data 1. Trajectory statistics for all tracked nucleosomes.

X and Y coordinates, distance between two steps, accumulated distance per trajectory, and angle between two steps are reported.

Figure supplement 2. The scatter plot of average step size over each frame of the videos shows no bias by the AFM tip, as the R^2 linear regression is 0.15.

Figure supplement 2—source data 1. Trajectory statistics for all tracked nucleosomes.

X and Y coordinates, distance between two steps, accumulated distance per trajectory, and angle between two steps are reported.

Figure supplement 2—source data 2. Basic statistics for all tracked nucleosomes.

Figure 2—video 1. HS-AFM video of in vitro reconstituted CENP-A chromatin in 5 mM NaCl containing buffer (low salt; speed =2 x).
https://elifesciences.org/articles/86709/figures#fig2video1

Figure 2—video 2. HS-AFM video of in vitro reconstituted CENP-A chromatin in 150 mM NaCl containing buffer (high salt; speed =2 x).
https://elifesciences.org/articles/86709/figures#fig2video2

Figure 2—video 3. HS-AFM video of in vitro reconstituted CENP-A chromatin imaged without functionalized mica (no APS; speed =2 x).
https://elifesciences.org/articles/86709/figures#fig2video3

Figure 2—video 4. HS-AFM video of in vitro reconstituted CENP-A chromatin imaged with double the amount of APS to functionalize mica (2 x APS; speed =2 x).
https://elifesciences.org/articles/86709/figures#fig2video4

Figure 2—video 5. HS-AFM video of in vitro reconstituted CENP-A chromatin imaged with physiological buffer +0.01% Tween (Tween; speed =2 x).
https://elifesciences.org/articles/86709/figures#fig2video5

Figure 2—video 6. HS-AFM video of in vitro reconstituted CENP-A chromatin on PCAT2 plasmid imaged with physiological buffer (DNA; speed =2 x).
https://elifesciences.org/articles/86709/figures#fig2video6

with positively charged amino groups, binding nucleic acid molecules under physiological conditions, allowing for the ability to image in air, in fluid, as well as perform force spectroscopy (*Lyubchenko et al., 2014*; *McAllister et al., 2005*; *Melters et al., 2019*; *Melters and Dalal, 2021*; *Rakshit et al., 2020*; *Shlyakhtenko et al., 2003*). We predicted that adding an excess of APS (333 nM APS is 2 x APS) would lower the diffusion constant compared to not adding APS (no APS). Indeed, we measured a lower diffusion constant for 2 x APS than no APS (*Figure 2D*, *Figure 2—source data 1 and 2*). If there were a tip effect, we reasoned there would be a difference in the diffusion constants between the x-axis and y-axis, which are parallel and perpendicular to the direction of tip scanning, respectively. We did not observe a bias in the diffusion constants between the two axes (*Figure 2D*; *Figure 2—figure supplement 1B*, *Figure 2—source data 1 and 2*). Third, to test for the potential impact of prolonged imaging on manipulation of trajectories, we assessed the step size distribution over time. We did not observe a significant effect of the video length on the step size (*Figure 2—figure supplement 2*, *Figure 2—source data 1 and 2*), indicating that extended imaging did not alter the trajectory dynamics. We are therefore confident that HS-AFM does not introduce a tip effect on chromatin and that drift is adequately corrected.

Salt and APS concentrations impact chromatin dynamics in an anticipated manner

Next, we set out to determine how different buffer conditions impact CENP-A chromatin dynamics. Different salt concentrations are known to impact chromatin compaction and dynamics (*Allahverdi et al., 2015*; *Brasch et al., 1971*; *Yager et al., 1989*; *Yager and van Holde, 1984*). At lower salt concentrations (below 50 mM NaCl), nucleosomes are stabilized, whereas at higher salt concentrations (above 100 mM NaCl) nucleosomes become unstable. Here, we tested the effect of low salt concentrations (5 mM NaCl) versus high salt concentration (150 mM NaCl) on nucleosome dynamics by HS-AFM. For each condition we tracked 124 and 161 nucleosome trajectories, respectively (*Table 1*, *Figure 3—videos 1 and 2*). As expected, the MSD curve for high salt had a larger slope than for low

Table 1. Quantifications of HS-AFM videos.

Either CENP-A or H3 nucleosomes were in vitro reconstituted on plasmid DNA and imaged in fluid in the presence or absence of either 2.2-fold excess CENP-C^{CD} or 0.2-fold excess of H1.5. *n*, number of nucleosome trajectories tracked. For each condition, at least three independent replicates were performed.

Sample	*n*	Number of steps	Average Diffusion constant (nm^2/s)	Average step size (nm)	Maximum R-step (nm)	R-step range (nm^2)
CENP-A nucleosomes	498	13,989	2.3±0.2	4.2±0.1	11.2±0.2	23.2±0.6
+1 x CENP-C^{CD}	368	7790	2.1±0.1	3.1±0.2	12.6±0.4	23.7±0.7
+2 x CENP-C^{CD}	310	9063	0.78±0.06	2.8±0.1	8.0±0.2	14.3±0.4
+4 x CENP-C^{CD}	166	7034	0.61±0.05	2.3±0.2	8.6±0.4	15.4±0.7
CENP-A controls						
Low salt	124	3783	1.2±0.2	2.8±0.1	9.6±0.4	18.3±0.9
High salt	161	4887	4.1±0.3	5.5±0.2	14.6±0.4	40±2
No APS	244	5186	7.5±0.5	6.0±2.0	15.9±0.4	43±2
2 x APS	120	2520	2.5±0.3	3.8±0.2	11.4±0.5	21±1
Tween-20	587	16,126	5.9±0.2	6.0±0.1	14.7±0.2	43±1
PCAT2 DNA	710	15,497	5.7±0.4	5.8±0.2	16.0±0.2	33.7±0.6
H3 controls						
H3 nucleosomes	66	1109	2.5±0.3	4.2±0.2	9.9±0.5	19±1
+H1.5	391	8492	3.2±0.3	4.7±0.1	12.3±0.3	26.9±0.8
H3 mononucleosome	90	1344	9.3±0.9	7.9±0.3	17.4±0.5	47±2

salt (*Figure 3A*, *Figure 3—figure supplement 1A*, *Figure 3—source data 1 and 2*). This is reflected in the diffusion constant, which was 1.2±0.2 nm^2·s^{-1} for low salt and 4.1±0.3 nm^2·s^{-1} for high salt (*Figure 3B*, *Figure 3—figure supplement 1B*, *Figure 3—source data 1 and 2*).

To better understand the step dynamics, we first assessed the average single-frame step size and found that the average step size of CENP-A nucleosomes for high salt is double the length of that of low salt (5.5±0.2 nm vs 2.8±0.1 nm, respectively, *Table 1*, *Figure 3—figure supplement 1C*, *Figure 3—source data 2*). Furthermore, we calculated the R-step. The R-step is the single-frame displacement in the plane of the trajectory and is defined as the square root of the sum of the squares of the displacement in the x and y directions. The maximum R-step was only slightly different between the low and high salt conditions (9.6±0.4 nm vs 14.5±0.4 nm, respectively, *Table 1*, *Figure 3—figure supplement 1D*, *Figure 3—source data 2*). When we looked at the total range of a trajectory by calculating the R-step range, we observed a much larger variance in the distribution for the high salt compared to the low salt (40±2 nm^2 vs 18.3±0.9 nm^2, respectively, *Table 1*, *Figure 2—figure supplement 1E*, *Figure 3—source data 2*). These results are in line with how salt concentration is known to impact chromatin dynamics (*Allahverdi et al., 2015*; *Brasch et al., 1971*; *Yager et al., 1989*; *Yager and van Holde, 1984*).

Next, we plotted the distributions of single step displacements in the x-axis and y-axis and fitted them to a single Gaussian distribution, which is expected for a diffusive process. Although the x- and y- single-step distributions were poorly fit by single Gaussian distributions (D_0), they were well-fit by a sum of two Gaussian distributions (D_1 and D_2) (*Figure 3D*, *Figure 3—figure supplements 2 and 3*, *Figure 3—source data 1 and 2*). The relative fraction of the two Gaussian distributions differed between low and high salt conditions (*Figure 3E*, *Figure 3—figure supplements 2 and 3*, *Figure 3—source data 1 and 2*). These data indicate that there are two distinct populations of nucleosomes in both low- and high-salt conditions. The D_1 Gaussian population represents slower diffusing nucleosomes, potentially reflecting transient pausing, whereas the D_2 Gaussian population represents faster diffusing nucleosomes. As AFM can only detect samples that are on the mica surface, one concern
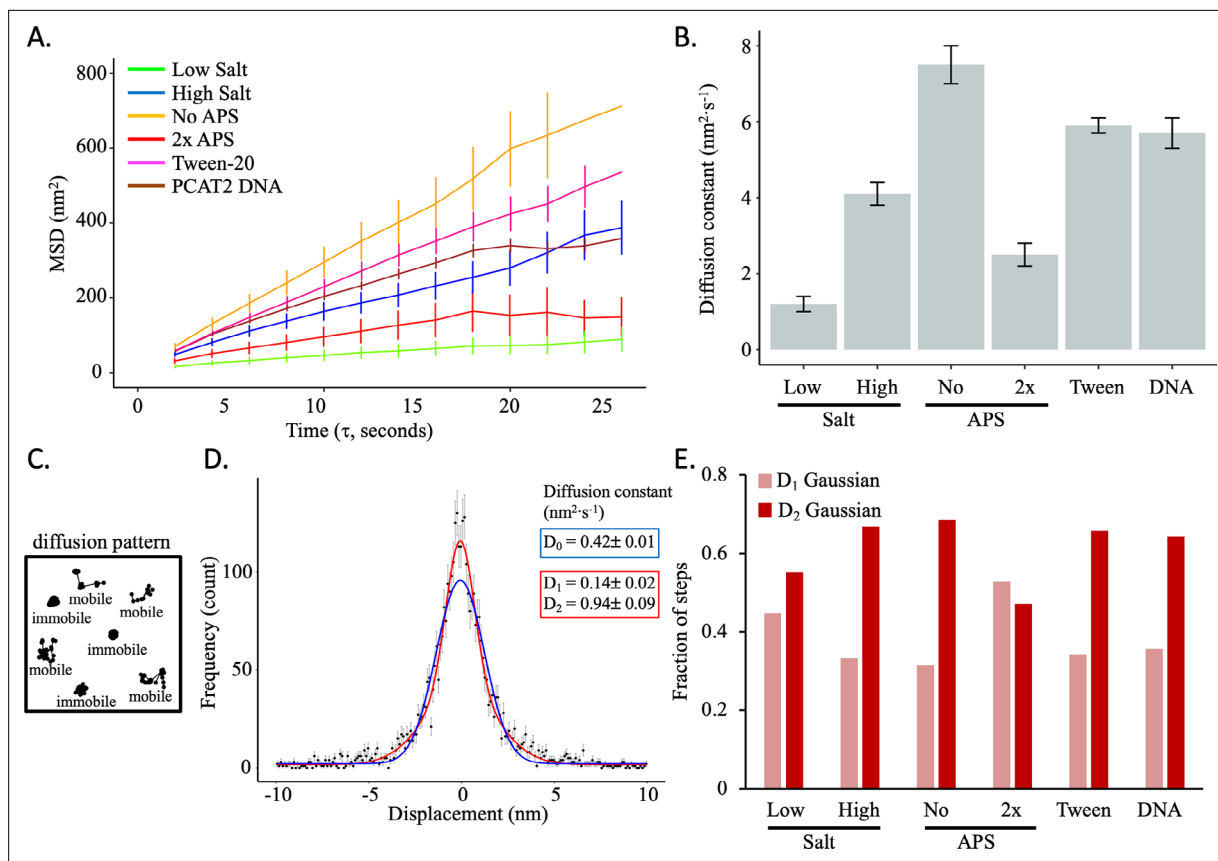
Figure 3. Salt and APS concentration predictably impacts CENP-A nucleosome mobility in vitro. (**A**) The average mean square displacement is shown with standard error as a function of the time interval for CENP-A nucleosome arrays in the following buffers: low salt (green; 5 mM NaCl), high salt (blue, 150 mM NaCl), no APS (yellow), twofold APS (red), 0.01% Tween-20 (pink), and PCAT2 DNA (brown). (**B**) The diffusion constants obtained from the MSD curves. The error bars represent the standard error. (**C**) Schematic representation of mobile or immobile (or paused) single particle trajectories. (**D**) The single step x-axis displacement of CENP-A nucleosomes in low salt conditions. The blue line represents a single Gaussian fit whereas the red line represents a double Gaussian fit. The latter provided a better fit to all the data for both the x- and y-step distributions for all conditions (see *Figure 3— figure supplement 5*). (**E**) The fraction of single steps corresponding to D_1 (narrower) Gaussian distribution or D_2 (wider) Gaussian distributions from the double Gaussian fitting. The D_1 Gaussian distribution corresponds to a smaller diffusion constant and may represent immobile or paused nucleosomes, whereas D_2 corresponds to a larger diffusion constant representing mobile nucleosomes. The data were obtained from two independent technical replicates per condition.

The online version of this article includes the following video, source data, and figure supplement(s) for figure 3:

Source data 1. Trajectory statistics for all tracked nucleosomes.

X and Y coordinates, distance between two steps, accumulated distance per trajectory, and angle between two steps are reported.

Source data 2. Basic statistics for all tracked nucleosomes.

Figure supplement 1. Impact of salt and APS concentration on step size statistics.

Figure supplement 1—source data 1. Trajectory statistics for all tracked nucleosomes.

X and Y coordinates, distance between two steps, accumulated distance per trajectory, and angle between two steps are reported.

Figure supplement 1—source data 2. Basic statistics for all tracked nucleosomes.

Figure supplement 2. Single (blue line) and double (red line) (sum of two) Gaussian fitting of the x and y step displacement distributions for each of the control conditions.

Figure supplement 2—source data 1. Trajectory statistics for all tracked nucleosomes.

X and Y coordinates, distance between two steps, accumulated distance per trajectory, and angle between two steps are reported.

Figure supplement 2—source data 2. Basic statistics for all tracked nucleosomes.

Figure supplement 3. The relative fraction of the D_1 and D_2 Gaussian fit are shown, where the D_2 (larger standard deviation, higher diffusion constant) Gaussian is most prevalent for all conditions except 2 x APS, Tween-20, and high salt.

Figure supplement 4. Individual tracts show switching between D_1 and D_2 diffusion states.

Figure 3 continued on next page

Figure 3 continued

Figure supplement 4—source data 1. Trajectory statistics for all tracked nucleosomes.

X and Y coordinates, distance between two steps, accumulated distance per trajectory, and angle between two steps are reported.

Figure supplement 5. Lower D_1 diffusion state and rejected "stuck" particles have different diffusion constants.

Figure supplement 5—source data 1. Basic statistics for the rejected 'stuck' trajectories, represented in *Figure 3—figure supplement 5*.

Figure supplement 6. Diffusion constant of H3 mononucleosomes higher than H3 nucleosomes within an array.

Figure supplement 6—source data 1. Trajectory statistics for all tracked nucleosomes.

X and Y coordinates, distance between two steps, accumulated distance per trajectory, and angle between two steps are reported.

Figure supplement 7. Single step distribution fit by single Gaussian for H3 mononucleosomes.

Figure supplement 7—source data 1. Basic statistics for all tracked nucleosomes.

Figure supplement 8. Schematic summary of the controls for HS-AFM quantitative single particle analysis.

Figure 3—video 1. HS-AFM video of in vitro reconstituted CENP-A chromatin in 5 mM NaCl containing buffer (low salt; speed =2 x).
https://elifesciences.org/articles/86709/figures#fig3video1

Figure 3—video 2. HS-AFM video of in vitro reconstituted CENP-A chromatin in 150 mM NaCl containing buffer (high salt; speed =2 x).
https://elifesciences.org/articles/86709/figures#fig3video2

Figure 3—video 3. HS-AFM video of in vitro reconstituted CENP-A chromatin imaged without functionalized mica (no APS; speed =2 x).
https://elifesciences.org/articles/86709/figures#fig3video3

Figure 3—video 4. HS-AFM video of in vitro reconstituted CENP-A chromatin imaged with double the amount of APS to functionalize mica (2 x APS; speed =2 x).
https://elifesciences.org/articles/86709/figures#fig3video4

Figure 3—video 5. HS-AFM video of in vitro reconstituted CENP-A chromatin imaged with physiological buffer +0.01% Tween (Tween; speed =2 x).
https://elifesciences.org/articles/86709/figures#fig3video5

Figure 3—video 6. HS-AFM video of in vitro reconstituted CENP-A chromatin on PCAT2 plasmid imaged with physiological buffer (DNA; speed =2 x).
https://elifesciences.org/articles/86709/figures#fig3video6

Figure 3—video 7. HS-AFM video of in vitro reconstituted H3 chromatin (speed =2 x).
https://elifesciences.org/articles/86709/figures#fig3video7

Figure 3—video 8. HS-AFM video of in vitro reconstituted H3 chromatin with H1.5, where H1.5 is added at a 0.2 molar ratio to H3 nucleosomes (speed =2 x).
https://elifesciences.org/articles/86709/figures#fig3video8

Figure 3—video 9. HS-AFM video of in vitro reconstituted H3 mononucleosomes (speed =2 x).
https://elifesciences.org/articles/86709/figures#fig3video9

might be that nucleosomes stick to the surface. To test for this possibility, we first manually verified whether individual nucleosomes could switch from what appears to be the smaller D_1 diffusion constant to the larger D_2 diffusion constant or vice versa. Indeed, we found a myriad of such examples across different conditions (*Figure 3—figure supplement 4A*). This was further reflected by the broad range of individual step sizes of each particle trajectory (*Figure 3—figure supplement 4B*, *Figure 3—source data 1*). Second, we tested whether the slower diffusing nucleosomes correspond to 'sticking' nucleosomes. To do this, we analyzed the rejected 'stuck' nucleosome trajectories with an average R-step of less than 1 nm and an R-step range of less than 8 nm. Next, we compared the effective diffusion constant of these 'stuck' nucleosomes for each video with the smaller diffusion constant obtained from the fit of a sum of two Gaussians. With the exception of the 2 x APS and low-salt conditions, we found that the effective diffusion constant of the 'stuck' nucleosome trajectories was significantly smaller than that of the smaller diffusion constant from the fit of a sum of two Gaussians (*Figure 3—figure supplement 5*, *Figure 3—figure supplement 5—source data 1*). In other words, these data would exclude the possibility of nucleosomes being 'stuck' to the mica surface.

Furthermore, the average step distribution (*Figure 3—figure supplement 1C*), maximum R-step (*Figure 3—figure supplement 1D*) and R-step range (*Figure 3—figure supplement 1E*) display a continuum of data points, instead of a bimodal distribution. Altogether, our data suggests that individual nucleosomes may have the capacity to move back and forth between the D_1 and the D_2 Gaussian distributions, indicating the possibility of switching between two diffusive modes.

Next, we expanded our analyses of the HS-AFM videos of the no APS and 2 x APS conditions (*Figure 3—videos 3 and 4*) to obtain the MSDs, and Gaussian fitting of the single step distributions. As APS functionalization positively charges the mica surface on which chromatin is deposited, we predicted that CENP-A nucleosomes trajectories would display faster dynamics in the no APS condition vs 2 x APS condition. Indeed, the slope of the MSD curve of in the absence of APS was larger compared to 2 x APS (*Figure 3A*, *Figure 3—figure supplement 1A*). The average diffusion constant was also higher in the absence of APS (7.5 ± 0.5 nm^2·s^{-1}) than 2 x APS (2.5 ± 0.3 nm^2·s^{-1}, *Figure 3B*, *Table 1*, *Figure 3—figure supplement 1B*, *Figure 3—source data 2*). A similar pattern was observed for the average step size (6.0 ± 2.0 nm vs 3.8 ± 0.2 nm, respectively), maximum R-step (15.9 ± 0.4 nm vs 11.4 ± 0.5 nm, respectively), and R-step variance (43 ± 2 nm^2 vs 21 ± 1 nm^2, respectively, *Table 1*, *Figure 3—figure supplement 1C–E*, *Figure 3—source data 2*), with higher values for no APS than 2 x APS. The single-step displacement distributions were well-fit by a sum of two Gaussians (*Figure 3—figure supplements 2 and 3*).

As an additional control, we used a very low concentration of Tween-20 (0.01%), a polysorbate surfactant that both stabilizes proteins and reduces non-specific hydrophobic interactions with the surface. We were interested to learn whether CENP-A chromatin in the presence of Tween-20 would display either more restricted nucleosomes mobility due to protein stabilization, or less restricted nucleosome mobility due to reduced non-specific interactions. HS-AFM videos of CENP-A chromatin in physiological buffer (0.5 x PBS, 2 mM MgCl$_2$) with 0.01% Tween-20 displayed the most amount of drift (*Figure 3—video 5*). After drift correction and filtering, we analyzed 587 trajectories to obtain single step distributions, MSD curves, and diffusion constants. We found that CENP-A chromatin in the presence of Tween-20 behaved more like no APS and high salt conditions with a steep MSD curve, a very broad distribution of average step sizes, and a large R-step range distribution (*Figure 3*, *Figure 3—figure supplements 1–3*, *Figure 3—source data 1 and 2*). We interpret this to mean that Tween-20 in the context of imaging CENP-A chromatin by HS-AFM primarily reduces non-specific hydrophobic interactions resulting in less restricted nucleosome mobility.

Furthermore, we wondered if our 3.5 kbp plasmid, which contains four copies of human centromere-derived α-satellite DNA, might induce nucleosome phasing or positioning (*Luger et al., 1997*; *Stormberg and Lyubchenko, 2022*). Therefore, we in vitro reconstituted CENP-A nucleosomes on an 8.5 kbp plasmid containing the lncRNA PCAT2 gene. In human cancer cell lines, ectopic CENP-A can be found at the PCAT2 locus, whereas, PCAT2 DNA is not known to position nucleosomes, in contrast to α-satellite DNA or the Widom 601-sequence (*Lowary and Widom, 1998*; *Luger et al., 1997*; *Stormberg and Lyubchenko, 2022*; *Thåström et al., 1999*). We observed an MSD curve similar to the high salt conditions (*Figure 3A*, *Figure 3—video 6*, *Figure 3—source data 1 and 2*), with an average diffusion constant of 5.7 ± 0.4 nm^2·s^{-1} (*Figure 3B*, *Table 1*, *Figure 3—source data 1 and 2*). A similar pattern was observed for the average step size (5.8 ± 0.2 nm), maximum R-step (16.0 ± 0.2 nm), and R-step variance (33.7 ± 0.6 nm^2, *Table 1*, *Figure 3—figure supplement 1C-E*, *Figure 3—source data 2*). The single step displacement distributions were well-fit by a sum of two Gaussians (*Figure 3—figure supplement 2*, *Figure 3—source data 1 and 2*). Overall, it appears that CENP-A nucleosomes reconstituted on the 8.5 kbp plasmid without known positioning sequences behaves similar to CENP-A nucleosomes reconstituted on 3.5 kbp plasmid with known positioning sequences, thereby suggesting that nucleosome mobility measured in these experiments may be independent of DNA sequence specificity.

When we analyzed previously published HS-AFM videos of H3 chromatin with or without linker histone H1.5 (*Melters and Dalal, 2021*) as well as H3 mononucleosomes, we observed a bias in both the angle between successive steps and Gaussian fitting of single step displacements (*Figure 3—figure supplements 6 and 7*, *Figure 3—videos 7–9*, *Figure 3—source data 1 and 2*). These data provide evidence that bias in HS-AFM trajectories is a possibility and that it can be detected. Furthermore, there was no difference in fitting either a single or double Gaussian distributions for H3 mononucleosomes (*Figure 3—figure supplement 7F*). Mononucleosomes are not associated with other nucleosomes and a priori mononucleosomes cannot display whole chromatin fiber motions, allowing mononucleosomes to move freely independent of the DNA strand. We observed that the diffusion constant of mononucleosomes is about threefold larger than that of chromatin arrays (*Table 1*) and 10- to 185-fold larger than the D$_1$ diffusion constants observed under various conditions (*Figure 3—figure supplements 2 and 7*). In addition, the R-step range of mononucleosomes is roughly twofold

larger than chromatin arrays (*Table 1*). Therefore, the latter observations imply that the unconstrained motion of mononucleosomes results in a single Gaussian distribution of step displacements.

Altogether, when we analyzed HS-AFM videos, CENP-A chromatin responded to varying salt and APS concentrations in agreement with previous reports (*Allahverdi et al., 2015*; *Brasch et al., 1971*; *Lyubchenko et al., 2014*; *Shlyakhtenko et al., 2003*; *Yager et al., 1989*; *Yager and van Holde, 1984*). Low salt and 2 x APS concentrations reduced CENP-A nucleosome mobility, whereas high salt and no APS concentrations increased CENP-A nucleosome mobility (*Figure 3—figure supplement 8*). For the remainder of the HS-AFM experiments, we used near physiological relevant salt concentrations (67.5 mM NaCl, 2 mM $MgCl_2$) and standardized APS concentrations (167 nM [*Lyubchenko et al., 2014*]).

CENP-C^{CD} represses CENP-A nucleosome mobility in vitro

Previously, we showed that a central domain fragment of CENP-C (*Figure 4A*) rigidified CENP-A nucleosomes and induced CENP-A nucleosome clustering (*Melters et al., 2019*). Based on these observations, we hypothesized that CENP-C^{CD} would reduce CENP-A nucleosome mobility. To test this hypothesis, we imaged CENP-A chromatin by HS-AFM under near physiological conditions. Subsequently, nucleosome tracks were extracted in either the absence (*Figure 4B*, *Figure 4—figure supplements 1–3*, *Figure 4—video 1*, *Figure 4—source data 1 and 2*) or presence of 1, 2, or 4 CENP-C^{CD} molecules (1 x, 2 x, or 4 x, respectively) per CENP-A nucleosome (*Figure 4C*, *Figure 4—figure supplements 1–3*, *Figure 4—videos 2–4*, *Figure 4—source data 1 and 2*). From at least 3 experiments per sample, we obtained 498, 368, 310, and 166 trajectories, respectively (*Table 1*). First, we verified that there were no motion artifacts associated with the tip scanning (*Figure 4—figure supplement 1*). Next, we calculated the MSD of CENP-A nucleosomes alone or in the presence of 1 x, 2 x, or 4 x CENP-C^{CD} and found that individual MSD curves of CENP-A nucleosomes were broadly distributed (*Figure 4D*, *Figure 4—figure supplement 2A*, B), with an average MSD curve that reached a plateau after ~25 s (*Figure 4—figure supplement 2A*), implying confined motion (*Kapanidis et al., 2018*; *Zhong and Wang, 2020*).

When CENP-C^{CD} was added at either 2 x or 4 x molar excess to CENP-A nucleosomes, CENP-A nucleosome mobility was strongly restricted (*Figure 4D*, *Figure 4—figure supplement 2A*, *Figure 4—videos 2–4*, *Figure 4—source data 1 and 2*). Indeed, the MSD curve was much lower for 2 x and 4 x CENP-C^{CD} compared to CENP-A alone, and the 2 x and 4 x CENP-C^{CD} MSD curve maintained a shallow slope (*Figure 4D*, *Figure 4—figure supplement 2A*). In contrast, the 1 x CENP-C^{CD} MSD curve was similar to CENP-A alone (*Figure 4D*, *Figure 4—figure supplement 2B*, *Figure 4—source data 1 and 2*). The diffusion constant of CENP-A alone was 2.3±0.2 nm²·s⁻¹, whereas the addition of 2 x and 4 x CENP-C^{CD} reduced the diffusion constant 2.9-fold to 0.78±0.06 nm²·s⁻¹ and 3.8-fold to 0.61±0.05 nm²·s⁻¹, respectively (*Table 1*, *Figure 4E*, *Figure 4—figure supplement 2B*, *Figure 4—source data 1 and 2*). This difference is reflected in the smaller single frame step size when CENP-C^{CD} is added to CENP-A chromatin compared to CENP-A chromatin alone (*Figure 4—figure supplement 2C*, *Figure 4—source data 2*). The maximum R-step and R-step range were also larger for CENP-A nucleosomes without CENP-C^{CD} (*Figure 4—figure supplement 2D*, E, *Figure 4—source data 2*). Next, we fitted the single step displacement distributions with Gaussian distributions and found that a sum of two Gaussian distributions provided better fits (*Figure 4—figure supplement 3*, *Figure 4—source data 1 and 2*). Overall, by HS-AFM we observed that CENP-C^{CD} restricts CENP-A nucleosome mobility in a switch-like manner. We hypothesized that this switch, as we recently observed (*Melters et al., 2019*), could be the mechanism by which overexpression of CENP-C in living cells results in CENP-A chromatin clustering.

Excess CENP-C suppresses centromeric RNAP2 levels and centromeric transcription in vivo

Next, we asked what the functional consequences are of CENP-C on CENP-A chromatin, beyond the formation of kinetochores (*Cheeseman et al., 2006*; *Walstein et al., 2021*; *Mendiburo et al., 2011*; *Régnier et al., 2005*). Previously, we showed that overexpressing CENP-C in HeLa cells resulted in increased clustering of centromeric chromatin and loss of centromeric RNAP2 (*Melters et al., 2019*). These results, combined with our 'decrease of motion' observations above, suggest that centromeric non-coding α-satellite transcription might be impaired in the background of CENP-C overexpression.
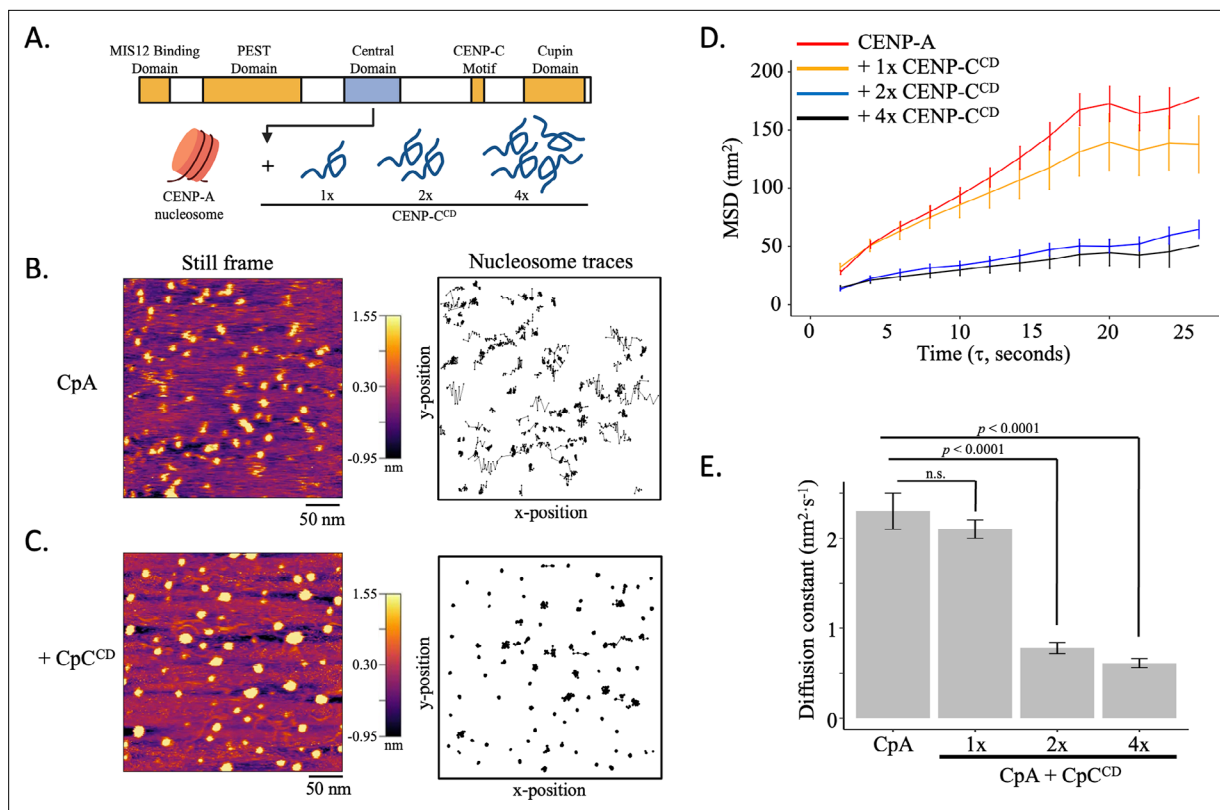
Figure 4. CENP-C^{CD} restrict CENP-A nucleosome mobility in vitro (**A**) Schematic representation of human CENP-C (943 amino acids: CENP-C, NCBI Gene ID: 1060). The central domain of CENP-C (CENP-C^{CD}), which directly binds to CENP-A nucleosomes, was added at a ratio of 1, 2, or 4 fragments per CENP-A nucleosome (1 x, 2 x, or 4 x CENP-C^{CD}, respectively). (**B**) CENP-A nucleosome arrays were tracked in fluid for up to 120 s by HS-AFM at 1 frame every 2 s. A representative still frame is shown as well as the trajectories over time. (**C**) CENP-A nucleosome arrays were tracked in the presence of 1 x, 2 x, or 4 x CENP-C^{CD}. A representative still frame is shown as well as the trajectories over time. (**D**) The average mean square displacement is shown with standard error as a function of the time interval. CENP-A nucleosomes alone are in red. CENP-A nucleosomes with 1 x CENP-C^{CD} is in yellow, 2 x CENP-C^{CD} is in blue, and 4 x CENP-C^{CD} is in black. (**E**) The diffusion constants obtained from the MSD curves. The line and bar graphs represent three independent technical replicates. The error bars represent the standard error.

The online version of this article includes the following video, source data, and figure supplement(s) for figure 4:

Source data 1. Trajectory statistics for all tracked nucleosomes.

X and Y coordinates, distance between two steps, accumulated distance per trajectory, and angle between two steps are reported.

Source data 2. Basic statistics for all tracked nucleosomes.

Figure supplement 1. The distribution of the angle between successive nucleosome positions for CENP-A chromatin alone or in the presence of 1 x, 2 x, or 4 x CENP-C^{CD}.

Figure supplement 2. CENP-C^{CD} restricts step size of CENP-A nucleosomes.

Figure supplement 2—source data 1. Trajectory statistics for all tracked nucleosomes.

Figure supplement 2—source data 2. Basic statistics for all tracked nucleosomes.

This includes diffusion constant (nm^2 ·s^{-1}), MSD slope (nm^2), average MSD slope (nm^2), average step size (nm), maximum R-step (nm), and R- step range (nm).

Figure supplement 3. CENP-C^{CD} does not impact double Gaussian of single step distribution of CENP-A nucleosomes.

Figure supplement 3—source data 1. Trajectory statistics for all tracked nucleosomes.

X and Y coordinates, distance between two steps, accumulated distance per trajectory, and angle between two steps are reported.

Figure supplement 3—source data 2. Basic statistics for all tracked nucleosomes.

Figure 4—video 1. HS-AFM video of in vitro reconstituted CENP-A chromatin (speed =2 x).

https://elifesciences.org/articles/86709/figures#fig4video1

Figure 4—video 2. HS-AFM video of in vitro reconstituted CENP-A chromatin with CENP-C^{CD} where CENP-C^{CD} is added at a 1 x molar ratio to CENP-A nucleosomes (speed =2 x).

Figure 4 continued on next page

To examine this facet of CENP-C:CENP-A homeostasis, we overexpressed CENP-C in HeLa cells to assess if centromeric transcription is altered.

First, we measured the effects of CENP-C overexpression on the level of RNAP2 on CENP-A chromatin. We overexpressed CENP-C 2.8-fold (*Figure 5—figure supplement 1*; *Figure 5—figure supplement 1—source data 1 and 2*) in HeLa cells for 72 hr and subsequently purified CENP-A chromatin associated with CENP-C by CENP-C native ChIP (nChIP), and the unbound CENP-A chromatin was pulled-down by sequential ACA nChIP. We found that RNAP2 levels were reduced upon CENP-C overexpression (*Figure 5A*, *Figure 5—figure supplement 1*, *Figure 5—figure supplement 1—source data 1 and 2*). In addition, we observed that, upon CENP-C overexpression, total CENP-A levels were also reduced (*Figure 5B*, *Figure 5—figure supplement 1*, *Figure 5—figure supplement 1—source data 1 and 2*). Previously (*Melters et al., 2019*), we showed that the addition of CENP-C^{CD} or overexpression of CENP-C results in compaction of CENP-A chromatin. We therefore wondered if CENP-C overexpression impacted centromeric transcription. By quantitative PCR, we observed
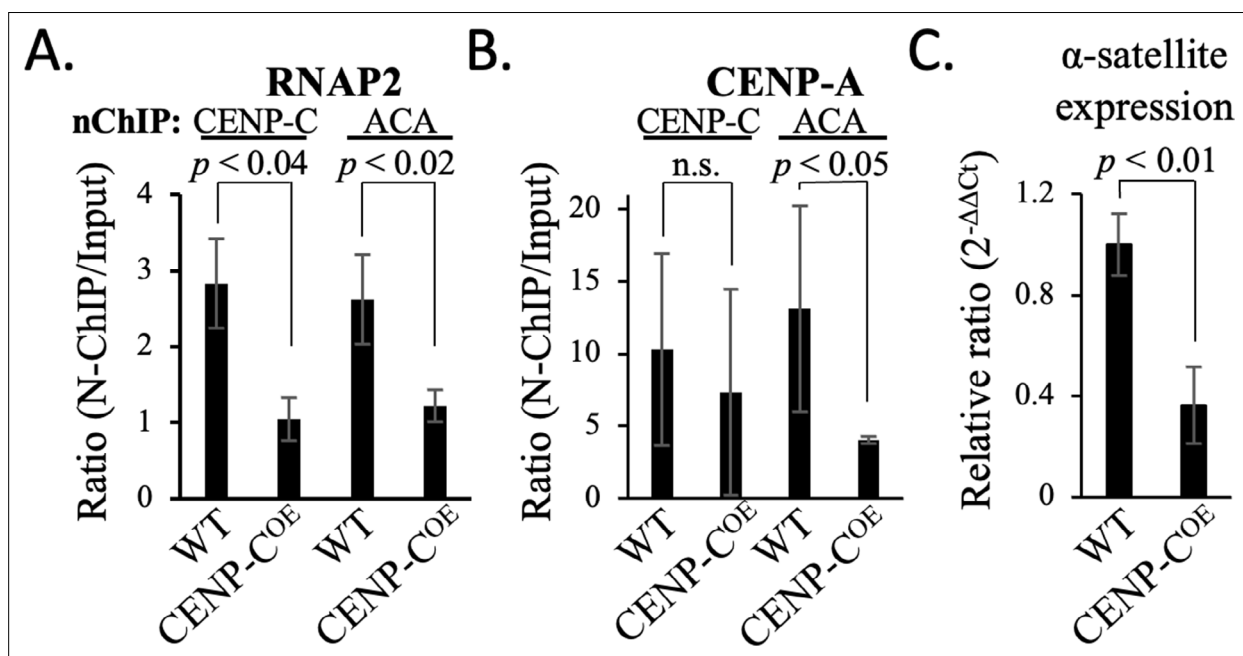

Figure 5. CENP-C overexpression suppressed α-satellite expression and centromeric RNAP2 occupancy. (**A**) Quantification of RNAP2 levels pulled down with either CENP-C or sequential ACA nChIP. (**B**) Quantification of CENP-A levels that pulled down with either CENP-C or sequential ACA nChIP. (**C**) Quantification of consensus α-satellite transcription in mock-transfected (WT) and CENP-C overexpression (CENP-C^{OE}) (two-sided t-test; significance was determined at p<0.05). The bar graphs represent three independent technical replicates, and the error bars represent standard deviations.

The online version of this article includes the following source data and figure supplement(s) for figure 5:

Source data 1. Quantification of RT-PCR of α-satellite transcripts for *Figure 5C*.

Figure supplement 1. Representative western blot quantifying RNAP2 and CENP-A levels.

Figure supplement 1—source data 1. Entire western blot as shown in Figure 5 – figure supplement 1.

Figure supplement 1—source data 2. Quantification of ChIP-western blot for Figures 5A, B.
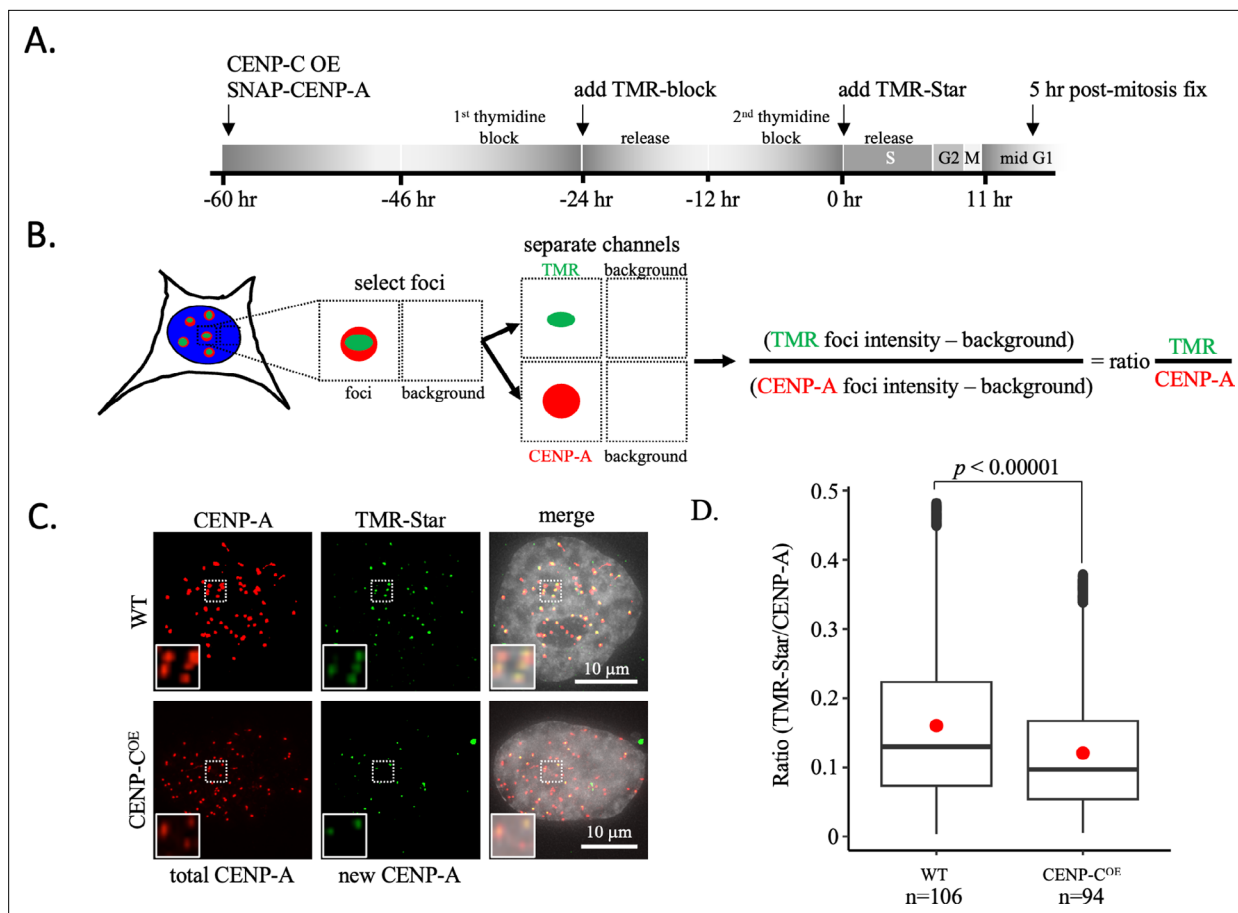
Figure 6. New CENP-A loading impaired upon CENP-C overexpression. (**A**) Schematic of experimental design. (**B**) Colocalized immunofluorescent signals for CENP-A and TMR-Star are collected and the intensity of both foci is measured as well as the background neighboring the foci to determine the ratio of the TMR-star signal over total CENP-A signal. (**C**) De novo CENP-A incorporation was assessed by quench pulse-chase immunofluorescence. After old CENP-A was quenched with TMR-block, newly loaded CENP-A was stained with TMR-Star and foci intensity was measured over total CENP-A foci intensity. Inset is a ×2 magnification of the dotted box in each respective image. (**D**) Quantification of de novo CENP-A loading by measuring the ratio of TMR-Star signal over total CENP-A signal (one-way ANOVA; significance was determined at p<0.05, n=number of cells analyzed). The box plots represent three independent technical replicates.

The online version of this article includes the following source data and figure supplement(s) for figure 6:

Figure supplement 1. Quantification of de novo CENP-A loading by measuring the ratio of TMR-Star signal over total CENP-A signal as shown in *Figure 6C* with individual data points.

Figure supplement 1—source data 1. Quantification of de novo CENP-A loading by measuring background corrected foci intensity for WT and CENP-C overexpressed cells.

a ~60% reduction in α-satellite transcripts in cells overexpressing CENP-C (*Figure 5C*, *Figure 5—source data 1*).

These results indicate that CENP-A levels are reduced and that centromeric transcription is indeed impaired upon CENP-C overexpression. Previous reports showed that new CENP-A loading is transcriptionally regulated (*Jansen et al., 2007*; *Quénet and Dalal, 2014*). Therefore, we hypothesized that CENP-C overexpression leads to defective de novo CENP-A loading.

CENP-C overexpression limits de novo CENP-A loading

To test this hypothesis, we turned to the well-established SNAP-tagged CENP-A system combined with quench pulse-chase immunofluorescence (*Bodor et al., 2012*). Using this system in cells synchronized to mid-G1, one can distinguish between older CENP-A (TMR-block) and newly incorporated CENP-A (TMR-Star; *Figure 6A and B*). Strikingly, in an CENP-C overexpression background, we

observed a 1.3-fold reduction of de novo incorporation of CENP-A (*Figure 6C and D*, *Figure 6—figure supplement 1—source data 1*).

Thus, the functional consequences of CENP-C overexpression are suppression of α-satellite transcription (*Figure 5C*) and subsequent impairment of new CENP-A loading (*Figure 6C and D*).

Discussion

Here, we demonstrate that HS-AFM is a reliable technique for studying single nucleosome dynamics by directly visualizing their motion in real time. Importantly, we show that the AFM tip scanning motion does not generate observable artifacts in nucleosome dynamics (*Figure 2*, *Figure 2—figure supplements 1 and 2*). Various critical scanning conditions were tested to assess their impact on CENP-A chromatin dynamics. Salt is a well-known factor that can either stabilize or destabilize chromatin (*Allahverdi et al., 2015*; *Brasch et al., 1971*; *Lyubchenko et al., 2014*; *Shlyakhtenko et al., 2003*; *Yager et al., 1989*; *Yager and van Holde, 1984*). Case in point, salt dialysis is a common method for in vitro nucleosome reconstitution (*Cruz-Becerra and Kadonaga, 2021*; *Peterson, 2008*; *Walkiewicz et al., 2014*). Indeed, low salt restricted CENP-A nucleosome motion, whereas high salt did the opposite (*Figure 3*, *Figure 3—figure supplements 1–3*). In AFM studies, APS is used to functionalize the mica surface with positive charges facilitating the interaction of DNA or chromatin with the mica surface. Not functionalizing the mica surface resulted in more mobile CENP-A nucleosomes, whereas 2 x APS functionalized mica resulted in increased levels of immobile CENP-A nucleosomes (*Figure 3*, *Figure 3—figure supplements 1–3*). Furthermore, we used a plasmid containing a non-nucleosome positioning sequence PCAT2 (*Figure 3*, *Figure 3—figure supplements 1–3*). Interestingly, the diffusion constant for CENP-A nucleosomes reconstituted on PCAT2 containing plasmid was higher than that of CENP-A nucleosomes reconstituted on α-satellite containing plasmid imaged under the same conditions (*Table 1*).There are various parameters that could account for this difference in diffusion constant. Only 20% of the α-satellite containing plasmid is comprised of nucleosome positioning sequences. Although it cannot be excluded, it is unlikely that the nucleosome positioning sequence reduces the global diffusion constants. Alternatively, the two plasmids differed substantially in length (8.5 kbp PCAT2 plasmid versus 3.5 kbp α-satellite plasmid). This means that PCAT2 plasmid possibly contained a much larger number of nucleosomes, potentially impacting local nucleosome density and thus chromatin compaction. The potential role of nucleosome crowding on nucleosome mobility should be investigated. In addition, H3 mononucleosomes were the only nucleosomes for which the single-frame step size distribution was well-fit by a single Gaussian (*Figure 3—figure supplement 7F*), this is in stark contrast with CENP-A chromatin, for which the step size distribution is well-fit by the sum of two Gaussians (*Figure 3—figure supplement 2*, *Figure 4—figure supplement 2*). This implies that nucleosome arrays might drive the two mobility states we observed. Looking more closely at individual tracks, we noticed that nucleosomes can switch between the D_1 and D_2 state (*Figure 3—figure supplement 3*). The slower D_1 diffusion constant did not appear to simply reflect nucleosomes being stuck to the mica surface (*Figure 3—figure supplement 5*). It will be interesting to learn what precisely causes the two Gaussian distributions, including whether oncohistones (*Nacev et al., 2019*), PTMs, or nucleosome binding factors (*Zhou et al., 2019*) can alter the relative probability of the two Gaussian distributions. Altogether, these data provide evidence that CENP-A nucleosomes respond to various control conditions in a predictable manner, but also that their dynamics are complex and include at least two mobility states.

CENP-C modulates both CENP-A nucleosome accessibility (*Ali-Ahmad et al., 2019*; *Ariyoshi et al., 2021*; *Falk et al., 2016*; *Falk et al., 2015*; *Guo et al., 2017*) and its elasticity (*Melters et al., 2019*). Here, we show that CENP-C^{CD} regulates CENP-A nucleosomes mobility in a switch-like manner (*Figure 4*, *Figure 4—figure supplements 1–3*). This might imply that CENP-C compacts CENP-A chromatin once a critical mass is reached. The data presented here correlates with CENP-C^{CD} rigidification of CENP-A nucleosomes (*Melters et al., 2019*). Additionally, we show that in vivo, CENP-C overexpression results in reduced levels of centromeric RNAP2 (*Melters et al., 2019*), impaired centromeric transcription (*Figure 5C*), and subsequent decreased loading of new CENP-A at the centromere (*Figure 6*). These findings combined provide evidence for a speculative link between the physical properties of nucleosomes, their mobility along DNA, and how these material properties might regulate chromatin accessibility and transcriptional potential.

In the nucleus, nucleosomes move in different dimensions, either in a single dimension along the DNA strand, or three dimensions where the DNA strand moves and the nucleosomes follow as passengers (*Babokhov et al., 2020*; *Ide et al., 2022*; *Melters and Dalal, 2021*). In addition, various events, ranging from transcription to DNA repair and replication, involve chromatin remodeling (*Nodelman and Bowman, 2021*; *Zaret, 2020*). Several in vivo studies have utilized tagged H2B combined with high-resolution live cell imaging to probe nucleosome dynamics. Nucleosomes within heterochromatin were less dynamic compared to euchromatin regions (*Ashwin et al., 2019*; *Maeshima et al., 2023*; *Nozaki et al., 2017*; *Ricci et al., 2015*), transcriptional inhibition diminished constraints of local chromatin movements (*Nagashima et al., 2019*), and local levels of H1 correlated with reduced nucleosome dynamics (*Gómez-García et al., 2021*). Indeed, chromatin-associated H1-eGFP mobility was two orders of magnitude smaller than free H1-eGFP (*Bernas et al., 2014*; *Wachsmuth et al., 2016*). ATP-driven effects also impact DNA motion (*Bhattacharya et al., 2006*; *Levi et al., 2005*). Tagging DNA is an effective method to test how mobile chromosome loci are in vivo. Using fluorescence recovery spectroscopy, GFP-tagged loci in CHO cells showed a slow and fast diffusion coefficient of $0.24 \cdot 10^{-3}$ and $3.13 \cdot 10^{-3}$ $\mu m^2 \cdot s^{-1}$ (*Levi et al., 2005*) and TetO tagged-DNA $D_H J_H$ loci in B cells had a diffusion coefficient of ~$2.0 \cdot 10^3$ $\mu m^2 \cdot s^{0.5}$ (*Lucas et al., 2014*). The change in diffusion coefficient of $V_H D_H$ loci is interpreted to results in a fourfold increase in interaction frequency (*Lucas et al., 2014*). In these cases, specific loci were tagged and tracked, but the behavior of individual nucleosomes within these domains remain unaccounted for. Therefore, in parallel, studies using optical tweezers probed the one dimensional diffusive behavior of nucleosomes (*Chen et al., 2019*; *Rudnizky et al., 2019*). A recent study using optical tweezers showed that the diffusion constant of H3 mononucleosomes sliding along a DNA strand is ~1.3 $bp^2 \cdot s^{-1}$ (~0.15 $nm^2 \cdot s^{-1}$; *Rudnizky et al., 2019*). This value is roughly similar to the D_1 diffusion constants we observed (*Figure 3—figure supplements 2 and 7*, *Figure 4—figure supplements 1 and 2*), implying that the D_1 diffusion constant might reflect sliding nucleosomes. Binding of transcription factors to nucleosomal DNA biases nucleosome motion, potentially through manipulation of the folding and unfolding of nucleosomal DNA around the nucleosome core particle (*Donovan et al., 2023*; *Rudnizky et al., 2019*). Here, we show that CENP-A nucleosomes have an average diffusion constant of 2.3±0.2 $nm^2 \cdot s^{-1}$ and their single-step distribution was well-fit by a sum of two Gaussian distributions (*Figure 4*, *Figure 4—figure supplement 2*). When CENP-C^{CD} was added at a two- or fourfold molar ratio to CENP-A nucleosomes, we observed a diffusion constant that is about three times lower than CENP-A nucleosomes alone (0.78±0.06 $nm^2 \cdot s^{-1}$ and 0.61±0.05 $nm^2 \cdot s^{-1}$, respectively). This difference in diffusion constants for nucleosomes between the Rudnizky study (~0.15 $nm^2 \cdot s^{-1}$, [*Rudnizky et al., 2019*]) and our results (0.61–2.3 $nm^2 \cdot s^{-1}$) could be due to technical differences of their experimental set-up compared to our experimental approach (optical tweezers vs HS-AFM). We used nucleosome arrays which permit both one-dimensional (nucleosome sliding) and two-dimensional motions (whole chromatin fiber movement) of nucleosomes compared to mononucleosomes that were fixed to polystyrene beads, which only permit one-dimensional motion (*Rudnizky et al., 2019*). In contrast, single molecule tracking in cultured cells captures nucleosome dynamics within the nucleus (*Iida et al., 2022*; *Kimura and Cook, 2001*; *Morisaki et al., 2014*; *Wagh et al., 2023*), but requires fluorophore-tags. Fluorophore-tags are photosensitive (*Jradi and Lavis, 2019*) and have the potential of altering the function of the protein it is bound to *Maheshwari et al., 2015*; *Ravi et al., 2010*. Calculated diffusion constants for H2B-eGFP range from 0.0019 $\mu m^2 \cdot s^{-1}$ to 7.3 $\mu m^2 \cdot s^{-1}$ (*Bhattacharya et al., 2006*; *Mazza et al., 2012*) and 0.03 $\mu m^2 \cdot s^{-1}$ to 1.39 $\mu m^2 \cdot s^{-1}$ for HALO-H2B (*Lovely et al., 2020*; *Ranjan et al., 2020*). These in vivo H2B diffusion constants are several orders of magnitudes larger than we observed (0.61–2.3 $nm^2 \cdot s^{-1}$). This could be due to the many activities within the nucleus of a living cell compared to the steady-state nature of an in vitro experiment. As such, the potential of single molecule analysis by HS-AFM to contribute to elegant studies in the field is exciting, as it can link single-molecule force spectroscopy analysis to in vivo single molecule tracking experiments.

Looking at another histone variant nucleosome, the diffusion constant of H2A.Z nucleosomes is larger than H3 nucleosomes (*Rudnizky et al., 2019*), which correlates with the transcriptional buffering function of H2A.Z (*Chen et al., 2019*; *Giaimo et al., 2019*). A logical prediction from our results would be that transcription through CENP-A chromatin would be more efficient compared to H3 chromatin. Indeed, a recent single-molecule study showed that CENP-A creates an open chromatin structure (*Nagpal and Fierz, 2022*). We found that proteins that exert their activity by binding to the outer
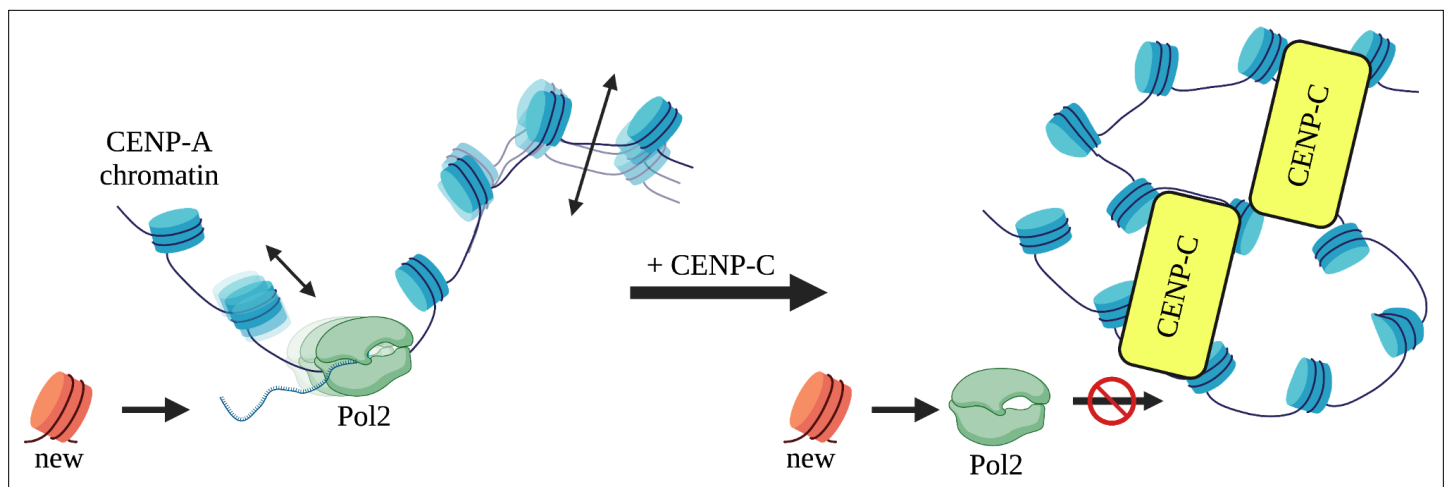
Figure 7. Clutch model for CENP-C restricted motion of CENP-A chromatin. Under wildtype conditions, we propose that CENP-A chromatin not bound by CENP-C (yellow box) forms a chromatin clutch and is readily accessible to the transcriptional machinery, because of the intrinsic material properties of CENP-A nucleosomes. In contrast, when CENP-C or CENP-C complexes bind CENP-A nucleosomes, a unique clutch of CENP-A chromatin is formed restricting sliding of CENP-A nucleosomes. This coincides with CENP-C^{CD} altering the material properties, and quenching the mobility, of CENP-A chromatin. Less mobile CENP-A nucleosomes restrict progression of the transcriptional machinery and subsequent loading of new CENP-A molecules.

surface of nucleosomes, rather than changing the internal constituents of nucleosomes, have the opposite effect on transcription. CENP-C^{CD} rigidifies CENP-A nucleosomes (*Melters et al., 2019*), and CENP-C^{CD}-CENP-A nucleosomes have a significantly reduced diffusion constant compared to CENP-A nucleosomes alone (*Table 1*). In vivo, overexpression of CENP-C resulted in decreased centromeric transcription (*Figure 6*). Thus, this study significantly extends the existing paradigm that suggests nucleosome dynamics are highly tunable, with a surprising twist – tuners can dampen or exaggerate nucleosome motion, which correlates with higher order chromatin folding and accessibility.

Taking these and prior findings in context, our data suggest a model where chromatin effector partners modify the material properties of histone variant nucleosomes at the local level, supporting the formation of functional nucleosome clutches (*Portillo-Ledesma et al., 2021*; *Ricci et al., 2015*; *Figure 7*). Here, we specifically probed CENP-A chromatin and based on our results we propose the following working model. CENP-A nucleosomes recruit CENP-C to form a kinetochore-promoting CENP-A chromatin clutch (*Kale et al., 2023*). CENP-C functions as the template for the recruitment of additional kinetochore proteins (*Klare et al., 2015*; *Yatskevich et al., 2023*). When CENP-C binds, CENP-A nucleosomes become rigidified (*Melters et al., 2019*) and restrict CENP-A nucleosomes mobility (*Figure 4*). This unique clutch facilitates the recruitment of other inner kinetochore components by locally immobilizing CENP-A chromatin (*Yatskevich et al., 2023*). Yet, to load new CENP-A molecules, transcription must happen (*Arunkumar and Melters, 2020*; *Quénet and Dalal, 2014*). The repressive chromatin state that CENP-C induces (*Figure 5*) contradicts this functional necessity. One speculative manner in which cells can work around the juxtaposition of the dual functions of CENP-A chromatin is by maintaining a pool of free centromeric CENP-A nucleosomes (*Figure 7*). Indeed, ChIP-seq and FISH data have established that centromeric CENP-C levels are lower compared to CENP-A levels (*Henikoff et al., 2015*; *Kyriacou and Heun, 2018*). We propose that unbound elastic and mobile CENP-A chromatin clutches create an intrinsically accessible chromatin state, allowing for the recruitment of transcriptional machinery that maintains centromeric CENP-A levels to facilitate both opposing functions (*Figure 7*). Succinctly, the epigenetic fate of a locus may be tightly, possibly causally, linked to the mechanical state of the chromatin fiber; concomitantly, the reinstatement of an epigenetic signature by de novo loading of a particular variant, reinforces the mechanical state of the fiber.

In summary, we report the MSDs and diffusion constants for CENP-A nucleosomes under a variety of conditions, and we show that single-step distributions are well-fit by the sum of two Gaussians. This implies that nucleosomes exist in at least two distinct mobility states. CENP-C^{CD} modulates centromeric chromatin by restricting the motions of CENP-A nucleosomes. As we observed a switch-like behavior of restricting CENP-A nucleosome motions, instead of a linear dose-response, we speculate

that CENP-C limits CENP-A mobility once a critical concentration is reached. In vivo, we observed diminished transcriptional competence when CENP-C is overexpressed, resulting in suppression of de novo CENP-A loading. These results strongly imply that there is a mechanistic link between modulating the material properties of nucleosomes and chromatin accessibility. Nucleosome dynamics play an important role in genome compaction and regulating DNA access by DNA binding factors. These dynamics are driven by only a few interactions between the interfaces of DNA and nucleosomes (*Fierz and Poirier, 2019*; *Polach and Widom, 1995*; *Widom, 1998*). An exciting line of investigation is to examine how at the nanoscale level the interaction between CENP-A nucleosomes and CENP-C protein co-evolved to repress CENP-A's mobile and elastic nature. It will also be crucial to examine how CENP-A:CENP-C homeostasis, along with those of other key inner kinetochore proteins such as CENP-N, T, S, X, and W regulate centromeric transcription and thereby de novo assembly of CENP-A to maintain the epigenetic identity of centromeres in other species. At a more global scale, it will be exciting to ask how different H1 variants modulate the chromatin fiber at the local level to promote or limit transcriptional competency, and how H1 variants dictate the mechanical motions of individual nucleosomes within the local 10 nm chromatin fiber.

Materials and methods

Key resources table

Reagent type (species) or resource	Designation	Source or reference	Identifiers	Additional information
Cell line (*Homo sapiens*)	HeLa (cervical carcinoma, Adult)	ATCC	CCL-2	
Antibody	Anti-CENP-A (Mouse monoclonal)	Abcam	Cat. #: ab13939, RRID: AB_300766	IF(1:1000)
Antibody	Anti-CENP-A (rabbit monoclonal)	Abcam	Cat. #: ab45694	WB (1:3000)
Antibody	Anti-CENP-C (guinea pig polyclonal)	MBL International	Cat. #: PD030, RRID: AB_10693556	nChIP (5 μL), WB (1:1000)
Antibody	Anti-CENP-C (rabbit polyclonal)	Santa Cruz	Cat. #: sc-22789	WB (1:500)
Antibody	Anti-H2A (rabbit polyclonal)	Abcam	Cat. #: ab18255, RRID: AB_470265	WB (1:1000)
Antibody	Anti-CENP-A (rabit polyclonal)	This paper		nChIP (3 μL per test)
Antibody	ACA serum (human, polyclonal)	BBI Solutions	SG140-2	nChIP (5 μL per test)
Recombinant DNA reagent	GFP-CENP-C (plasmid)	Gift from Stephan Diekmann		pGFP-CENP-C (KAN)
Recombinant DNA reagent	SNAP-CENP-A (plasmid)	This paper		SNAP version of pCh-C-CENP-A (AMP)
Recombinant DNA reagent	PCAT2 (plasmid)	*Arunkumar et al., 2022*		
Recombinant DNA reagent	4 x α-satellite (plasmid)	*Quénet and Dalal, 2014*		
Sequence-based reagent	Centromeric α-satellite_F	*Quénet and Dalal, 2014*	PCR primers	CATCACAAAGAAGTTTCTGAGAATGCTTC
Sequence-based reagent	Centromeric α-satellite_R	*Quénet and Dalal, 2014*	PCR primers	TGCATTCAACTCACAGAGTTGAACCTTCC
Sequence-based reagent	GAPDH_F	*Quénet and Dalal, 2014*	PCR primers	GCGGTTCCGCACATCCCGGTAT
Sequence-based reagent	GAPDH_R	*Quénet and Dalal, 2014*	PCR primers	CCCCACGTCGCAGCTTGCCTA

Continued on next page

Continued

Reagent type (species) or resource	Designation	Source or reference	Identifiers	Additional information
Peptide, recombinant protein	CENP-A/H4 tetramer	EpiCypher	Cat. #: 16–010	
Peptide, recombinant protein	H2A/H2B dimer	EpiCypher	Cat. #: 15–0311	
Peptide, recombinant protein	H3/H4 tetramer	EpiCypher	Cat. #: 16–0008	
Commercial assay or kit	TMR-Block	New England Biolabs	Cat. #: S9106S	
Commercial assay or kit	TMR-Star	New England Biolabs	Cat. #: S9105S	
Commercial assay or kit	NeonTM Transfection System 100 µL kit	ThermoFisher Scientific	Cat. #: MPK10025	
Software, algorithm	R	https://www.r-project.org/	RRID:SCR_002865	
Software, algorithm	Gwyddion	http://gwyddion.net/	RRID: SCR_015583	
Software, algorithm	NIH ImageJ	https://imagej.net/software/fiji/	RRID: SCR_003070	
Software, algorithm	ggplot2	https://cran.r-project.org/web/packages/ggplot2/index.html	RRID: SCR_014601	
Software, algorithm	CRaQ	http://facilities.igc.gulbenkian.pt/microscopy/microscopy-macros.php		
Software, algorithm	Adobe Photostop	https://www.adobe.com/products/photoshop.html	RRID: SCR_014199	
Software, algorithm	MATLAB	https://www.mathworks.com/products/matlab.html	RRID: SCR_001622	
Software, algorithm	MatLabTrack	https://sourceforge.net/projects/single-molecule-tracking/		
Other	Vectashield with DAPI	Vector Laboratories	H-1200	Stain nuclei

In vitro reconstitution

In vitro reconstitution of CENP-A (CENP-A/H4 cat#16–010 and H2A/H2B cat#15–0311, EpiCypher, Research Triangle Park, NC) and H3 (H3/H4 cat#16–0008 and H2A/H2B cat#15–0311, EpiCypher Research Triangle Park, NC) nucleosomes were in vitro reconstituted on either 3.5 kbp plasmid containing four copies of α-satellite DNA or a 8.5 kbp plasmid containing 3 copies of PCAT2 lncRNA gene performed as previously described (*Dimitriadis et al., 2010*; *Walkiewicz et al., 2014*). For quality purposes, an aliquot of each sample was imaged by AFM in non-contact tapping mode, before moving on to high-speed AFM.

High-speed AFM

In vitro reconstituted CENP-A and H3 chromatin with the addition of CENP-C[CD] (*Melters et al., 2019*) or H1.5 (*Melters and Dalal, 2021*), respectively was imaged with the Cypher VRS (Oxford Instruments, Asylum Research, Santa Barbara, CA) using ultra-small silicon cantilevers (BL-AC10DS with nominal resonances of ~1500 kHz, stiffness of ~0.1 N/m) in non-contact-mode. The V1-grade mica on top of the scanning pilar was peeled and functionalized with 167 nM APS, before 10 µL of sample was added. The sample was incubated for 15–20 minutes before initializing scanning to obtain a density of ~400 nucleosome/µm². The sample was imaged at a speed of 268.82 Hz (frame rate = 1 Hz or one frame per second) and a resolution of 512x256 points and lines for an area of 400x400 nm (CENP-A and CENP-A +CENP C[CD] samples with a nucleosome density of ~300 nucleosomes/µm², respectively), 300x300 nm (H3 +H1.5 sample with a nucleosome density of ~200 nucleosomes/µm²),

and 250x250 nm (H3 sample with a nucleosome density of ~200 nucleosomes/μm^2). As the AFM tip moves from the top of the scan area to the bottom, before moving back up again. This cycle repeats itself. This means that the relative tip location on the scan area between successive images do not perfectly correspond in time. To avoid getting inaccurate tracking data, we limited our analysis to only every other scanned image to guarantee that the relative tip position between two successive analyzed images. Videos were saved in mp4 format, converted to TIFF sequences using Photoshop (Adobe), prepared for single molecule tracking in ImageJ (Fuji), and tracked with MATLAB's Matlab-Track v6.0 package. Obtained nucleosome tracks that were shorter than 10 frames and had single steps exceeding 24 nm or nucleosome tracks with average R-step less than 1 nm and a maximum R-range less than 8 nm were excluded from the analysis. Using ggplot2 package in R (version 4.2.1), drift was visualized and calculated for each individual video and any observed drift was corrected and verified. The remaining nucleosome tracks were subsequently analyzed to obtain the mean square displacement curves, diffusion constant, angle between successive frames, single frame step sizes, the maximum R-step, and R-step range. The R-step is the single-frame displacement in the plane. It is defined as the square root of the sum of the squares of the displacement in the x and y direction [R-step = $\sqrt{(\Delta x^2 + \Delta y^2)}$]. The results were visualized using the ggplot2 package in R (version 4.2.1). The diffusion constant for each nucleosome sample was estimated from the initial two points of each MSD (*Vestergaard et al., 2014*). The mean and standard error of the mean are reported as the diffusion constant and uncertainty for each nucleosome sample. The mean diffusion constant is identical to the diffusion constant derived from the first two points of the average MSD curves for each nucleosome sample. To test whether the smaller D_1 diffusion constant is indistinguishable from 'stuck' or rejected particle trajectories, we compared the x-axis and y-axis diffusion constants of the 'stuck' particle trajectories to the D_1 diffusion constant. We fitted the rejected steps in the x- and y- directions to a single Gaussian distribution and obtained the diffusion constant from the standard deviation of the fitted Gaussian. The effective diffusion constants of the 'stuck' trajectories were compared to the smaller D_1 diffusion constant. We used the F-test to compare the Gaussian variances to determine the probability that the smaller D_1 diffusion constant is consistent with the 'stuck' particle trajectories. The diffusion constants and step analyses were performed in a double-blind manner.

Native chromatin immunoprecipitation and western blotting

HeLa cells (CCL-2 from AATC; tested negative for mycoplasma contamination) were grown in DMEM (Invitrogen/ThermoFisher Cat #11965) supplemented with 10% FBS and 1 X penicillin and strepto-mycin cocktail. nChIP experiments were performed without fixation. After cells were grown to ~80% confluency, they were harvested as described (*Bui et al., 2017*; *Bui et al., 2012*). For best results, the pellet obtained for chromatin was spun-down during the nuclei extraction protocol (*Walkiewicz et al., 2014*) and was broken up with a single gentle tap. Nuclei were digested for 6 minutes with 0.25 U MNase/mL (Sigma-Aldrich cat #N3755-500UN) and supplemented with 1.5 mM $CaCl_2$. Following quenching (10 mM EGTA), nuclei pellets were spun down, and chromatin was extracted gently, over-night in an end-over-end rotator, in low salt solution (0.5 x PBS; 0.1 mM EGTA; protease inhibitor cock-tail (Roche cat #05056489001)). nChIP chromatin bound to Protein G Sepharose beads (GE Healthcare cat #17-0618-02) were gently washed twice with ice cold 0.5 x PBS and spun down for 1 min at 4 °C at 800 rpm. Following the first nChIP, the unbound fraction was used for the sequential nChIP. Western analyses were done using LiCor's Odyssey CLx scanner and Image Studio v2.0.

Quantitative PCR

α-satellite expression levels in HeLa cells that were either mock transfected or transfected GFP-CENP-C (generous gift from Stephan Diekmann) using the Neon Transfection System 100 μL kit (Cat. #: MPK10025, Thermo Fisher Scientific, Waltham, MA) per instructions (*McNulty et al., 2017*; *Quénet and Dalal, 2014*). RNA was extracted, quantified by UV-spectroscopy, and equal quantities were retro-transcribed using Superscript III First-Strand Synthesis kit as described above. Complemen-tary DNA (cDNA) samples were prepared using the iQ SYBR Green supermix (#170–8880; Biorad) following manufacturer's protocol. Control reactions without cDNA were performed to rule out non-specific amplification. The quantitative PCR was run on 'Step one plus Real time PCR' system (Applied Biosystem, Grand Island, NY). Primer sequences are:

The comparative cycle threshold (C_T) method was used to analyze the expression level of α-satellite transcripts. C_T values were normalized against the average C_T value of the housekeeping gene GAPDH. Relative fold differences ($2^{-\Delta\Delta CT}$) are indicated in *Figure 5C*.

Quench pulse-chase immunofluorescence

To quantify de novo assembled CENP-A particles, we transfected HeLa cells with SNAP-tagged CENP-A under a CMV promoter in combination with either empty vector or GFP-CENP-C (generous gift from Stephan Diekmann) using the Neon Transfection System 100 µL kit (Cat. #: MPK10025, Thermo Fisher Scientific, Waltham, MA) per instructions. The quench pulse-chase experiment was performed according to *Bodor et al., 2012*. In short, following transfection, cells were synchronized with double thymidine block. At the first release TMR-block (S9106S, New England Biolabs, Ipswich, MA) was added per manufactures instruction and incubated for 30 min at 37 °C, followed by three washes with cell culture media. At the second release TMR-Star (S9105S, New England Biolabs, Ipswich, MA) was added per manufactures instructions and incubated for 30 min at 37 °C, followed by three washes with cell culture media. Fourteen hours after adding TMR-Star, cells were fixed with 1% paraformaldehyde in PEM (80 mM K-PIPES pH 6.8, 5 mM EGTA pH 7.0, 2 mM $MgCl_2$) for 10 min at RT. Next, cells were washed three times with ice cold PEM. To extract soluble proteins, cells were incubated with 0.5% Triton-X in CSK (10 mM K-PIPES pH 6.8, 100 mM NaCl, 300 mM sucrose, 3 mM $MgCl_2$, 1 mM EGTA) for 5 min at 4 °C. The cells were rinsed with PEM and fixed for a second time with 4% PFA in PEM for 20 min at 4 °C. Next, the cells were washed three times with PEM. Next, the cells were incubated in blocking solution (1 X PBS, 3% BSA, 5% normal goat serum) for 1 hr at RT. CENP-A antibody (ab13979 1:1000) was added for 1 hr at RT, followed by three washes with 1 X PBS-T and a 10 min incubation with blocking solution at RT. Anti-mouse secondary (Alexa-488 1:1000) was added for 1 hr at RT, followed by three 1 X PBS-T and two 1 X PBS washes. Following air-drying, cells were mounted with Vectashield with DAPI (H-1200, Vector Laboratories, Burlingame, CA) and the coverslips were sealed with nail polish. Images were collected using a DeltaVision RT system fitted with a CoolSnap charged-coupled device camera and mounted on an Olympus IX70. Deconvolved IF images were processed using ImageJ. From up to 22 nuclei, colocalizing CENP-A and TMR-Star foci signal were collected, as well as directly neighboring regions using the CRaQ ImageJ macro (*Bodor et al., 2012*). Background signal intensity was subtracted from corresponding CENP-A and TMR-Star signal intensity before the ratio CENP-A/TMR-Star was determined using the CRaQ ImageJ macro (*Bodor et al., 2012*). Samples were imaged in a double-blind manner. Graphs were prepared using the ggplot2 package for R (version 4.2.1).

Quantification and statistical analyses

Significant differences for western blot quantification and nucleosome track measurements from HS-AFM analyses were performed using either paired or two-sided t-test, F-test, or one-way ANOVA as described in the Figure legends. Significance was determined at $p < 0.05$.

Acknowledgements

Additional information

Competing interests

Yamini Dalal: Reviewing editor, eLife. The other authors declare that no competing interests exist.

Author ORCIDs

Daniël P Melters (i) https://orcid.org/0000-0003-4809-0562
Keir C Neuman (i) http://orcid.org/0000-0002-0863-5671
Yamini Dalal (i) http://orcid.org/0000-0002-7655-6182

Additional files

Supplementary files

• MDAR checklist

Data availability

All data generated and analyzed during this study are included in the manuscript and supporting files; Source data files have been provided for Figures 1-6 and accompanied Figure 1-6 - figure supplements. Entire western blot shown in Figure 1 - figure supplement 1 - source data 1 and Figure 5 - figure supplement 1 - source data 1 are included.

References

Ali-Ahmad A, Bilokapić S, Schäfer IB, Halić M, Sekulić N. 2019. CENP-C unwraps the human CENP-A nucleosome through the H2A C-terminal tail. *EMBO Reports* **20**:e48913. DOI: https://doi.org/10.15252/embr.201948913, PMID: 31475439

Allahverdi A, Chen Q, Korolev N, Nordenskiöld L. 2015. Chromatin compaction under mixed salt conditions: opposite effects of sodium and potassium ions on nucleosome array folding. *Scientific Reports* **5**:8512. DOI: https://doi.org/10.1038/srep08512, PMID: 25688036

Allshire RC, Madhani HD. 2018. Ten principles of heterochromatin formation and function. *Nature Reviews. Molecular Cell Biology* **19**:229–244. DOI: https://doi.org/10.1038/nrm.2017.119, PMID: 29235574

Ando T. 2018. High-speed atomic force microscopy and its future prospects. *Biophysical Reviews* **10**:285–292. DOI: https://doi.org/10.1007/s12551-017-0356-5, PMID: 29256119

Ariyoshi M, Makino F, Watanabe R, Nakagawa R, Kato T, Namba K, Arimura Y, Fujita R, Kurumizaka H, Okumura E-I, Hara M, Fukagawa T. 2021. Cryo-EM structure of the CENP-A nucleosome in complex with phosphorylated CENP-C. *The EMBO Journal* **40**:e105671. DOI: https://doi.org/10.15252/embj.2020105671, PMID: 33463726

Arunkumar G, Melters DP. 2020. Centromeric transcription: a conserved swiss-army knife. *Genes* **11**:911. DOI: https://doi.org/10.3390/genes11080911, PMID: 32784923

Arunkumar G, Baek S, Sturgill D, Bui M, Dalal Y. 2022. Oncogenic lncRNAs alter epigenetic memory at a fragile chromosomal site in human cancer cells. *Science Advances* **8**:eabl5621. DOI: https://doi.org/10.1126/sciadv.abl5621, PMID: 35235361

Ashwin SS, Nozaki T, Maeshima K, Sasai M. 2019. Organization of fast and slow chromatin revealed by single-nucleosome dynamics. *PNAS* **116**:19939–19944. DOI: https://doi.org/10.1073/pnas.1907342116

Babokhov M, Hibino K, Itoh Y, Maeshima K. 2020. Local chromatin motion and transcription. *Journal of Molecular Biology* **432**:694–700. DOI: https://doi.org/10.1016/j.jmb.2019.10.018, PMID: 31689435

Bannister AJ, Zegerman P, Partridge JF, Miska EA, Thomas JO, Allshire RC, Kouzarides T. 2001. Selective recognition of methylated lysine 9 on histone H3 by the HP1 chromo domain. *Nature* **410**:120–124. DOI: https://doi.org/10.1038/35065138, PMID: 11242054

Bernas T, Brutkowski W, Zarębski M, Dobrucki J. 2014. Spatial heterogeneity of dynamics of H1 linker histone. *European Biophysics Journal* **43**:287–300. DOI: https://doi.org/10.1007/s00249-014-0962-0, PMID: 24830851

Bhattacharya D, Mazumder A, Miriam SA, Shivashankar GV. 2006. EGFP-tagged core and linker histones diffuse via distinct mechanisms within living cells. *Biophysical Journal* **91**:2326–2336. DOI: https://doi.org/10.1529/biophysj.105.079343, PMID: 16815908

Bodor DL, Rodríguez MG, Moreno N, Jansen LET. 2012. Analysis of protein turnover by quantitative SNAP-based pulse-chase imaging. *Current Protocols in Cell Biology* United states: John Wiley and Sons. DOI: https://doi.org/10.1002/0471143030.cb0808s55, PMID: 23129118

Brasch K, Seligy VL, Setterfield G. 1971. Effects of low salt concentration on structural organization and template activity of chromatin in chicken erythrocyte nuclei. *Experimental Cell Research* **65**:61–72. DOI: https://doi.org/10.1016/s0014-4827(71)80050-2, PMID: 5549552

Bui M, Dimitriadis EK, Hoischen C, An E, Quénet D, Giebe S, Nita-Lazar A, Diekmann S, Dalal Y. 2012. Cell-cycle-dependent structural transitions in the human CENP-A nucleosome in vivo. *Cell* **150**:317–326. DOI: https://doi.org/10.1016/j.cell.2012.05.035, PMID: 22817894

Bui M, Pitman M, Nuccio A, Roque S, Donlin-Asp PG, Nita-Lazar A, Papoian GA, Dalal Y. 2017. Internal modifications in the CENP-A nucleosome modulate centromeric dynamics. *Epigenetics & Chromatin* **10**:17. DOI: https://doi.org/10.1186/s13072-017-0124-6

Bury L, Moodie B, Ly J, McKay LS, Miga KH, Cheeseman IM. 2020. Alpha-satellite RNA transcripts are repressed by centromere-nucleolus associations. *eLife* **9**:e59770. DOI: https://doi.org/10.7554/eLife.59770, PMID: 33174837

Buschbeck M, Hake SB. 2017. Variants of core histones and their roles in cell fate decisions, development and cancer. *Nature Reviews. Molecular Cell Biology* **18**:299–314. DOI: https://doi.org/10.1038/nrm.2016.166, PMID: 28144029

Bustamante CJ, Chemla YR, Liu S, Wang MD. 2021. Optical tweezers in single-molecule biophysics. *Nature Reviews. Methods Primers* **1**:25. DOI: https://doi.org/10.1038/s43586-021-00021-6, PMID: 34849486

Cheeseman IM, Chappie JS, Wilson-Kubalek EM, Desai A. 2006. The conserved KMN network constitutes the core microtubule-binding site of the kinetochore. *Cell* **127**:983–997. DOI: https://doi.org/10.1016/j.cell.2006.09.039, PMID: 17129783

Chen Z, Gabizon R, Brown AI, Lee A, Song A, Díaz-Celis C, Kaplan CD, Koslover EF, Yao T, Bustamante C. 2019. High-resolution and high-accuracy topographic and transcriptional maps of the nucleosome barrier. *eLife* **8**:e48281. DOI: https://doi.org/10.7554/eLife.48281, PMID: 31364986

Chien F-T, van Noort J. 2009. 10 years of tension on chromatin: results from single molecule force spectroscopy. *Current Pharmaceutical Biotechnology* **10**:474–485. DOI: https://doi.org/10.2174/138920109788922128, PMID: 19689315

Chung YC, Bisht M, Thuma J, Tu LC. 2023. Single-chromosome dynamics reveals locus-dependent dynamics and chromosome territory orientation. *Journal of Cell Science* **136**:jcs260137. DOI: https://doi.org/10.1242/jcs.260137, PMID: 36718642

Cruz-Becerra G, Kadonaga JT. 2021. Reconstitution of chromatin by Stepwise salt dialysis. *Bio-Protocol* **11**:e3977. DOI: https://doi.org/10.21769/BioProtoc.3977, PMID: 33889671

DeLuca JG, Musacchio A. 2012. Structural organization of the kinetochore-microtubule interface. *Current Opinion in Cell Biology* **24**:48–56. DOI: https://doi.org/10.1016/j.ceb.2011.11.003, PMID: 22154944

Dimitriadis EK, Weber C, Gill RK, Diekmann S, Dalal Y. 2010. Tetrameric organization of vertebrate centromeric nucleosomes. *PNAS* **107**:20317–20322. DOI: https://doi.org/10.1073/pnas.1009563107, PMID: 21059934

Donovan BT, Luo Y, Meng Z, Poirier MG. 2023. The nucleosome unwrapping free energy landscape defines distinct regions of transcription factor accessibility and kinetics. *Nucleic Acids Research* **51**:1139–1153. DOI: https://doi.org/10.1093/nar/gkac1267, PMID: 36688297

Escobar TM, Loyola A, Reinberg D. 2021. Parental nucleosome segregation and the inheritance of cellular identity. *Nature Reviews. Genetics* **22**:379–392. DOI: https://doi.org/10.1038/s41576-020-00312-w, PMID: 33500558

Falk SJ, Guo LY, Sekulic N, Smoak EM, Mani T, Logsdon GA, Gupta K, Jansen LET, Van Duyne GD, Vinogradov SA, Lampson MA, Black BE. 2015. CENP-C reshapes and stabilizes CENP-A nucleosomes at the centromere. *Science* **348**:699–703. DOI: https://doi.org/10.1126/science.1259308, PMID: 25954010

Falk S.J, Lee J, Sekulic N, Sennett MA, Lee TH, Black BE. 2016. CENP-C directs A structural transition of CENP-A nucleosomes mainly through sliding of DNA gyres. *Nature Structural & Molecular Biology* **23**:204–208. DOI: https://doi.org/10.1038/nsmb.3175

Fierz B, Poirier MG. 2019. Biophysics of chromatin dynamics. *Annual Review of Biophysics* **48**:321–345. DOI: https://doi.org/10.1146/annurev-biophys-070317-032847, PMID: 30883217

Flamm WG, Walker PMB, McCallum M. 1969. Some properties of the single strands isolated from the DNA of the nuclear satellite of the mouse (*Mus musculus*). *Journal of Molecular Biology* **40**:423–443. DOI: https://doi.org/10.1016/0022-2836(69)90163-6, PMID: 5364715

Giaimo BD, Ferrante F, Herchenröther A, Hake SB, Borggrefe T. 2019. The histone variant H2A.Z in gene regulation. *Epigenetics & Chromatin* **12**:37. DOI: https://doi.org/10.1186/s13072-019-0274-9

Gómez-García PA, Portillo-Ledesma S, Neguembor MV, Pesaresi M, Oweis W, Rohrlich T, Wieser S, Meshorer E, Schlick T, Cosma MP, Lakadamyali M. 2021. Mesoscale modeling and single-nucleosome tracking reveal

remodeling of clutch folding and dynamics in stem cell differentiation. *Cell Reports* **34**:108614. DOI: https://doi.org/10.1016/j.celrep.2020.108614, PMID: 33440158

Guo LY, Allu PK, Zandarashvili L, McKinley KL, Sekulic N, Dawicki-McKenna JM, Fachinetti D, Logsdon GA, Jamiolkowski RM, Cleveland DW, Cheeseman IM, Black BE. 2017. Centromeres are maintained by fastening CENP-A to DNA and directing an arginine anchor-dependent nucleosome transition. *Nature Communications* **8**:15775. DOI: https://doi.org/10.1038/ncomms15775, PMID: 28598437

Hara M, Ariyoshi M, Sano T, Nozawa RS, Shinkai S, Onami S, Jansen I, Hirota T, Fukagawa T. 2023. Centromere/kinetochore is assembled through CENP-C oligomerization. *Molecular Cell* **83**:2188–2205.. DOI: https://doi.org/10.1016/j.molcel.2023.05.023

Henikoff JG, Thakur J, Kasinathan S, Henikoff S. 2015. A unique chromatin complex occupies young α-satellite arrays of human centromeres. *Science Advances* **1**:e1400234. DOI: https://doi.org/10.1126/sciadv.1400234, PMID: 25927077

Hwang KK, Eissenberg JC, Worman HJ. 2001. Transcriptional repression of euchromatic genes by *Drosophila* heterochromatin protein 1 and histone modifiers. *PNAS* **98**:11423–11427. DOI: https://doi.org/10.1073/pnas.211303598, PMID: 11562500

Ide S, Tamura S, Maeshima K. 2022. Chromatin behavior in living cells: Lessons from single-nucleosome imaging and tracking. *BioEssays* **44**:e2200043. DOI: https://doi.org/10.1002/bies.202200043, PMID: 35661389

Iida S, Shinkai S, Itoh Y, Tamura S, Kanemaki MT, Onami S, Maeshima K. 2022. Single-nucleosome imaging reveals steady-state motion of interphase chromatin in living human cells. *Science Advances* **8**:eabn5626. DOI: https://doi.org/10.1126/sciadv.abn5626, PMID: 35658044

Izeddin I, Récamier V, Bosanac L, Cissé II, Boudarene L, Dugast-Darzacq C, Proux F, Bénichou O, Voituriez R, Bensaude O, Dahan M, Darzacq X. 2014. Single-molecule tracking in live cells reveals distinct target-search strategies of transcription factors in the nucleus. *eLife* **3**:e02230. DOI: https://doi.org/10.7554/eLife.02230, PMID: 24925319

Jamge B, Lorković ZJ, Axelsson E, Osakabe A, Shukla V, Yelagandula R, Akimcheva S, Kuehn AL, Berger F. 2023. Histone variants shape chromatin states in Arabidopsis. *eLife* **12**:RP87714. DOI: https://doi.org/10.7554/eLife.87714, PMID: 37467143

Jansen LET, Black BE, Foltz DR, Cleveland DW. 2007. Propagation of centromeric chromatin requires exit from mitosis. *The Journal of Cell Biology* **176**:795–805. DOI: https://doi.org/10.1083/jcb.200701066, PMID: 17339380

Janssen A, Colmenares SU, Karpen GH. 2018. Heterochromatin: guardian of the genome. *Annual Review of Cell and Developmental Biology* **34**:265–288. DOI: https://doi.org/10.1146/annurev-cellbio-100617-062653, PMID: 30044650

Jradi FM, Lavis LD. 2019. Chemistry of photosensitive fluorophores for single-molecule localization microscopy. *ACS Chemical Biology* **14**:1077–1090. DOI: https://doi.org/10.1021/acschembio.9b00197, PMID: 30997987

Kale S, Boopathi R, Belotti E, Lone IN, Graies M, Schröder M, Petrova M, Papin C, Bednar J, Ugrinova I, Hamiche A, Dimitrov S. 2023. The CENP-A nucleosome: where and when it happens during the inner kinetochore's assembly. *Trends in Biochemical Sciences*:S0968-0004(23)00176-7. DOI: https://doi.org/10.1016/j.tibs.2023.07.010, PMID: 37596196

Kapanidis AN, Uphoff S, Stracy M. 2018. Understanding protein mobility in Bacteria by tracking single molecules. *Journal of Molecular Biology* **430**:4443–4455. DOI: https://doi.org/10.1016/j.jmb.2018.05.002, PMID: 29753778

Killian JL, Ye F, Wang MD. 2018. Optical tweezers: a force to be reckoned with. *Cell* **175**:1445–1448. DOI: https://doi.org/10.1016/j.cell.2018.11.019, PMID: 30500527

Kimura H, Cook PR. 2001. Kinetics of core histones in living human cells: little exchange of H3 and H4 and some rapid exchange of H2B. *The Journal of Cell Biology* **153**:1341–1353. DOI: https://doi.org/10.1083/jcb.153.7.1341, PMID: 11425866

Klare K, Weir JR, Basilico F, Zimniak T, Massimiliano L, Ludwigs N, Herzog F, Musacchio A. 2015. CENP-C is a blueprint for constitutive centromere–associated network assembly within human kinetochores. *Journal of Cell Biology* **210**:11–22. DOI: https://doi.org/10.1083/jcb.201412028

Klemm SL, Shipony Z, Greenleaf WJ. 2019. Chromatin accessibility and the regulatory epigenome. *Nature Reviews Genetics* **20**:207–220. DOI: https://doi.org/10.1038/s41576-018-0089-8

Kyriacou E, Heun P. 2018. High-resolution mapping of centromeric protein association using APEX-chromatin fibers. *Epigenetics & Chromatin* **11**:68. DOI: https://doi.org/10.1186/s13072-018-0237-6

Lachner M, O'Carroll D, Rea S, Mechtler K, Jenuwein T. 2001. Methylation of histone H3 lysine 9 creates a binding site for HP1 proteins. *Nature* **410**:116–120. DOI: https://doi.org/10.1038/35065132, PMID: 11242053

Levi V, Ruan Q, Plutz M, Belmont AS, Gratton E. 2005. Chromatin dynamics in interphase cells revealed by tracking in a two-photon excitation microscope. *Biophysical Journal* **89**:4275–4285. DOI: https://doi.org/10.1529/biophysj.105.066670, PMID: 16150965

Lovely GA, Braikia FZ, Singh A, Schatz DG, Murre C, Liu Z, Sen R. 2020. Direct Observation of RAG Recombinase Recruitment to Chromatin and the *IgH* Locus in Live pro-B Cells. *bioRxiv*. DOI: https://doi.org/10.1101/2020.09.07.286484

Lowary PT, Widom J. 1998. New DNA sequence rules for high affinity binding to histone octamer and sequence-directed nucleosome positioning. *Journal of Molecular Biology* **276**:19–42. DOI: https://doi.org/10.1006/jmbi.1997.1494, PMID: 9514715

Lucas JS, Zhang Y, Dudko OK, Murre C. 2014. 3D trajectories adopted by coding and regulatory DNA elements: first-passage times for genomic interactions. *Cell* **158**:339–352. DOI: https://doi.org/10.1016/j.cell.2014.05.036, PMID: 24998931

Luger K, Mäder AW, Richmond RK, Sargent DF, Richmond TJ. 1997. Crystal structure of the nucleosome core particle at 2.8 A resolution. *Nature* **389**:251–260. DOI: https://doi.org/10.1038/38444, PMID: 9305837

Lyubchenko YL, Gall AA, Shlyakhtenko LS. 2014. Visualization of DNA and protein–DNA complexes with atomic force microscopy in. Kuo J (Ed). *Electron Microscopy: Methods and Protocols* Totowa, NJ: Humana Press. p. 367–384. DOI: https://doi.org/10.1007/978-1-62703-776-1

Maeshima K, Ide S, Babokhov M. 2019. Dynamic chromatin organization without the 30-nm fiber. *Current Opinion in Cell Biology* **58**:95–104. DOI: https://doi.org/10.1016/j.ceb.2019.02.003, PMID: 30908980

Maeshima K, Iida S, Shimazoe MA, Tamura S, Ide S. 2023. Is euchromatin really open in the cell? Trends in Cell Biology. *Trends Cell Biol* S0962–S8924. DOI: https://doi.org/10.1016/j.tcb.2023.05.007

Maheshwari S, Tan EH, West A, Franklin FCH, Comai L, Chan SWL, Bomblies K. 2015. Naturally occurring differences in CENH3 affect chromosome segregation in zygotic mitosis of hybrids. *PLOS Genetics* **11**:e1004970. DOI: https://doi.org/10.1371/journal.pgen.1004970, PMID: 25622028

Martire S, Banaszynski LA. 2020. The roles of histone variants in fine-tuning chromatin organization and function. *Nature Reviews. Molecular Cell Biology* **21**:522–541. DOI: https://doi.org/10.1038/s41580-020-0262-8, PMID: 32665685

Mazza D, Abernathy A, Golob N, Morisaki T, McNally JG. 2012. A benchmark for chromatin binding measurements in live cells. *Nucleic Acids Research* **40**:e119. DOI: https://doi.org/10.1093/nar/gks701, PMID: 22844090

McAllister C, Karymov MA, Kawano Y, Lushnikov AY, Mikheikin A, Uversky VN, Lyubchenko YL. 2005. Protein interactions and misfolding analyzed by AFM force spectroscopy. *Journal of Molecular Biology* **354**:1028–1042. DOI: https://doi.org/10.1016/j.jmb.2005.10.012, PMID: 16290901

McNulty SM, Sullivan LL, Sullivan BA. 2017. Human Centromeres produce chromosome-specific and array-specific Alpha Satellite transcripts that are complexed with CENP-A and CENP-C. *Developmental Cell* **42**:226–240.. DOI: https://doi.org/10.1016/j.devcel.2017.07.001, PMID: 28787590

Melters DP, Nye J, Zhao H, Dalal Y. 2015. Chromatin dynamics in Vivo: a game of musical chairs. *Genes* **6**:751–776. DOI: https://doi.org/10.3390/genes6030751, PMID: 26262644

Melters DP, Pitman M, Rakshit T, Dimitriadis EK, Bui M, Papoian GA, Dalal Y. 2019. Intrinsic elasticity of nucleosomes is encoded by histone variants and calibrated by their binding partners. *PNAS* **116**:24066–24074. DOI: https://doi.org/10.1073/pnas.1911880116

Melters DP, Dalal Y. 2021. Nano-Surveillance: tracking individual molecules in a Sea of Chromatin. *Journal of Molecular Biology* **433**:166720. DOI: https://doi.org/10.1016/j.jmb.2020.11.019, PMID: 33221335

Mendiburo MJ, Padeken J, Fülöp S, Schepers A, Heun P. 2011. *Drosophila* CENH3 is sufficient for centromere formation. *Science* **334**:686–690. DOI: https://doi.org/10.1126/science.1206880, PMID: 22053052

Morisaki T, Müller WG, Golob N, Mazza D, McNally JG. 2014. Single-molecule analysis of transcription factor binding at transcription sites in live cells. *Nature Communications* **5**:4456. DOI: https://doi.org/10.1038/ncomms5456, PMID: 25034201

Mueller F, Stasevich TJ, Mazza D, McNally JG. 2013. Quantifying transcription factor kinetics: at work or at play? *Critical Reviews in Biochemistry and Molecular Biology* **48**:492–514. DOI: https://doi.org/10.3109/10409238.2013.833891, PMID: 24025032

Nacev BA, Feng L, Bagert JD, Lemiesz AE, Gao JJ, Soshnev AA, Kundra R, Schultz N, Muir TW, Allis CD. 2019. The expanding landscape of "oncohistone" mutations in human cancers. *Nature* **567**:473–478. DOI: https://doi.org/10.1038/s41586-019-1038-1, PMID: 30894748

Nagashima R, Hibino K, Ashwin SS, Babokhov M, Fujishiro S, Imai R, Nozaki T, Tamura S, Tani T, Kimura H, Shribak M, Kanemaki MT, Sasai M, Maeshima K. 2019. Single nucleosome imaging reveals loose genome chromatin networks via active RNA polymerase II. *The Journal of Cell Biology* **218**:1511–1530. DOI: https://doi.org/10.1083/jcb.201811090, PMID: 30824489

Nagpal H, Fierz B. 2022. CENP-A and CENP-B Collaborate to Create an Open Centromeric Chromatin State. *bioRxiv*. DOI: https://doi.org/10.1101/2022.07.08.499316

Nakayama J, Rice JC, Strahl BD, Allis CD, Grewal SIS. 2001. Role of Histone H3 Lysine 9 Methylation in epigenetic control of heterochromatin assembly. *Science* **292**:110–113. DOI: https://doi.org/10.1126/science.1060118

Neuman KC, Nagy A. 2008. Single-molecule force spectroscopy: optical tweezers, magnetic tweezers and atomic force microscopy. *Nature Methods* **5**:491–505. DOI: https://doi.org/10.1038/nmeth.1218, PMID: 18511917

Nodelman IM, Bowman GD. 2021. Biophysics of Chromatin Remodeling. *Annual Review of Biophysics* **50**:73–93. DOI: https://doi.org/10.1146/annurev-biophys-082520-080201, PMID: 33395550

Nozaki T, Imai R, Tanbo M, Nagashima R, Tamura S, Tani T, Joti Y, Tomita M, Hibino K, Kanemaki MT, Wendt KS, Okada Y, Nagai T, Maeshima K. 2017. Dynamic organization of chromatin domains revealed by super-resolution live-cell imaging. *Molecular Cell* **67**:282–293.. DOI: https://doi.org/10.1016/j.molcel.2017.06.018, PMID: 28712725

Peterson CL. 2008. Salt gradient dialysis reconstitution of nucleosomes. *CSH Protocols* **2008**:db. DOI: https://doi.org/10.1101/pdb.prot5113, PMID: 21356758

Polach KJ, Widom J. 1995. Mechanism of protein access to specific DNA sequences in Chromatin: a dynamic equilibrium model for Gene Regulation. *Journal of Molecular Biology* **254**:130–149. DOI: https://doi.org/10.1006/jmbi.1995.0606

Portillo-Ledesma S, Tsao LH, Wagley M, Lakadamyali M, Cosma MP, Schlick T. 2021. Nucleosome clutches are regulated by Chromatin internal parameters. *Journal of Molecular Biology* **433**:166701. DOI: https://doi.org/10.1016/j.jmb.2020.11.001, PMID: 33181171

Przewloka MR, Zhang W, Costa P, Archambault V, D'Avino PP, Lilley KS, Laue ED, McAinsh AD, Glover DM. 2007. Molecular analysis of core kinetochore composition and assembly in *Drosophila melanogaster*. *PLOS ONE* **2**:e478. DOI: https://doi.org/10.1371/journal.pone.0000478, PMID: 17534428

Quénet D, Dalal Y. 2014. A long non-coding RNA is required for targeting centromeric protein A to the human centromere. *eLife* **3**:e03254. DOI: https://doi.org/10.7554/eLife.03254, PMID: 25117489

Rakshit T, Melters DP, Dimitriadis EK, Dalal Y. 2020. Mechanical properties of nucleoprotein complexes determined by nanoindentation spectroscopy. *Nucleus* **11**:264–282. DOI: https://doi.org/10.1080/19491034.2020.1816053, PMID: 32954931

Ranjan A, Nguyen VQ, Liu S, Wisniewski J, Kim JM, Tang X, Mizuguchi G, Elalaoui E, Nickels TJ, Jou V, English BP, Zheng Q, Luk E, Lavis LD, Lionnet T, Wu C. 2020. Live-cell single particle imaging reveals the role of RNA polymerase II in histone H2A.Z eviction. *eLife* **9**:e55667. DOI: https://doi.org/10.7554/eLife.55667, PMID: 32338606

Ravi M, Kwong PN, Menorca RMG, Valencia JT, Ramahi JS, Stewart JL, Tran RK, Sundaresan V, Comai L, Chan SWL. 2010. The rapidly evolving centromere-specific histone has stringent functional requirements in *Arabidopsis thaliana*. *Genetics* **186**:461–471. DOI: https://doi.org/10.1534/genetics.110.120337, PMID: 20628040

Régnier V, Vagnarelli P, Fukagawa T, Zerjal T, Burns E, Trouche D, Earnshaw W, Brown W. 2005. CENP-A is required for accurate chromosome segregation and sustained kinetochore association of BubR1. *Molecular and Cellular Biology* **25**:3967–3981. DOI: https://doi.org/10.1128/MCB.25.10.3967-3981.2005, PMID: 15870271

Ricci MA, Manzo C, García-Parajo MF, Lakadamyali M, Cosma MP. 2015. Chromatin fibers are formed by heterogeneous groups of nucleosomes in vivo. *Cell* **160**:1145–1158. DOI: https://doi.org/10.1016/j.cell.2015.01.054, PMID: 25768910

Rothbart SB, Strahl BD. 2014. Interpreting the language of histone and DNA modifications. *Biochimica et Biophysica Acta (BBA) - Gene Regulatory Mechanisms* **1839**:627–643. DOI: https://doi.org/10.1016/j.bbagrm.2014.03.001

Rudnizky S, Khamis H, Malik O, Melamed P, Kaplan A. 2019. The base pair-scale diffusion of nucleosomes modulates binding of transcription factors. *PNAS* **116**:12161–12166. DOI: https://doi.org/10.1073/pnas.1815424116

Sanulli S, Trnka MJ, Dharmarajan V, Tibble RW, Pascal BD, Burlingame AL, Griffin PR, Gross JD, Narlikar GJ. 2019. HP1 reshapes nucleosome core to promote phase separation of heterochromatin. *Nature* **575**:390–394. DOI: https://doi.org/10.1038/s41586-019-1669-2, PMID: 31618757

Schultz J. 1936. Variegation in *Drosophila* and the inert chromosome regions. *PNAS* **22**:27–33. DOI: https://doi.org/10.1073/pnas.22.1.27

Shen H, Tauzin LJ, Baiyasi R, Wang W, Moringo N, Shuang B, Landes CF. 2017. Single particle tracking: from Theory to Biophysical Applications. *Chemical Reviews* **117**:7331–7376. DOI: https://doi.org/10.1021/acs.chemrev.6b00815, PMID: 28520419

Shlyakhtenko LS, Miloseska L, Potaman VN, Sinden RR, Lyubchenko YL. 2003. Intersegmental interactions in supercoiled DNA: atomic force microscope study. *Ultramicroscopy* **97**:263–270. DOI: https://doi.org/10.1016/S0304-3991(03)00051-2, PMID: 12801679

Specht EA, Braselmann E, Palmer AE. 2017. A critical and comparative review of Fluorescent Tools for live-cell imaging. *Annual Review of Physiology* **79**:93–117. DOI: https://doi.org/10.1146/annurev-physiol-022516-034055, PMID: 27860833

Stormberg T, Lyubchenko YL. 2022. The sequence dependent Nanoscale structure of CENP-A Nucleosomes. *International Journal of Molecular Sciences* **23**:11385. DOI: https://doi.org/10.3390/ijms231911385, PMID: 36232691

Taverna SD, Li H, Ruthenburg AJ, Allis CD, Patel DJ. 2007. How chromatin-binding modules interpret histone modifications: lessons from professional pocket pickers. *Nature Structural & Molecular Biology* **14**:1025–1040. DOI: https://doi.org/10.1038/nsmb1338

Thåström A, Lowary PT, Widlund HR, Cao H, Kubista M, Widom J. 1999. Sequence motifs and free energies of selected natural and non-natural nucleosome positioning DNA sequences. *Journal of Molecular Biology* **288**:213–229. DOI: https://doi.org/10.1006/jmbi.1999.2686, PMID: 10329138

Tolsma TO, Hansen JC. 2019. Post-translational modifications and chromatin dynamics. *Essays in Biochemistry* **63**:89–96. DOI: https://doi.org/10.1042/EBC20180067, PMID: 31015385

van Staalduinen J, van Staveren T, Grosveld F, Wendt KS. 2023. Live-cell imaging of chromatin contacts opens a new window into chromatin dynamics. *Epigenetics & Chromatin* **16**:27. DOI: https://doi.org/10.1186/s13072-023-00503-9

Vestergaard CL, Blainey PC, Flyvbjerg H. 2014. Optimal estimation of diffusion coefficients from single-particle trajectories. *Physical Review E* **89**:022726. DOI: https://doi.org/10.1103/PhysRevE.89.022726

Wachsmuth M, Knoch TA, Rippe K. 2016. Dynamic properties of independent chromatin domains measured by correlation spectroscopy in living cells. *Epigenetics & Chromatin* **9**:57. DOI: https://doi.org/10.1186/s13072-016-0093-1

Wagh K, Stavreva DA, Jensen RAM, Paakinaho V, Fettweis G, Schiltz RL, Wüstner D, Mandrup S, Presman DM, Upadhyaya A, Hager GL. 2023. Dynamic switching of transcriptional regulators between two distinct low-mobility chromatin states. *Science Advances* **9**:eade1122. DOI: https://doi.org/10.1126/sciadv.ade1122, PMID: 37315128

Walkiewicz MP, Bui M, Quénet D, Dalal Y. 2014. Tracking histone variant nucleosomes across the human cell cycle using biophysical, biochemical, and cytological analyses. *Methods in Molecular Biology* **1170**:589–615. DOI: https://doi.org/10.1007/978-1-4939-0888-2_34, PMID: 24906339

Walstein K, Petrovic A, Pan D, Hagemeier B, Vogt D, Vetter IR, Musacchio A. 2021. Assembly principles and stoichiometry of a complete human kinetochore module. *Science Advances* **7**:eabg1037. DOI: https://doi.org/10.1126/sciadv.abg1037, PMID: 34193424

Wang Z, Wang X, Zhang Y, Xu W, Han X. 2021. Principles and applications of single particle tracking in cell research. *Small* **17**:e2005133. DOI: https://doi.org/10.1002/smll.202005133, PMID: 33533163

Weintraub H, Groudine M. 1976. Chromosomal subunits in active genes have an altered conformation. *Science* **193**:848–856. DOI: https://doi.org/10.1126/science.948749, PMID: 948749

Weir JR, Faesen AC, Klare K, Petrovic A, Basilico F, Fischböck J, Pentakota S, Keller J, Pesenti ME, Pan D, Vogt D, Wohlgemuth S, Herzog F, Musacchio A. 2016. Insights from biochemical reconstitution into the architecture of human kinetochores. *Nature* **537**:249–253. DOI: https://doi.org/10.1038/nature19333

Widom J. 1998. Structure, dynamics, and function of chromatin in vitro. *Annual Review of Biophysics and Biomolecular Structure* **27**:285–327. DOI: https://doi.org/10.1146/annurev.biophys.27.1.285, PMID: 9646870

Wu C, Wong YC, Elgin SCR. 1979. The chromatin structure of specific genes: II. Disruption of chromatin structure during gene activity. *Cell* **16**:807–814. DOI: https://doi.org/10.1016/0092-8674(79)90096-5, PMID: 455450

Yager TD, van Holde KE. 1984. Dynamics and equilibria of nucleosomes at elevated ionic strength. *The Journal of Biological Chemistry* **259**:4212–4222 PMID: 6707002.

Yager TD, McMurray CT, van Holde KE. 1989. Salt-induced release of DNA from nucleosome core particles. *Biochemistry* **28**:2271–2281. DOI: https://doi.org/10.1021/bi00431a045, PMID: 2719953

Yatskevich S, Barford D, Muir KW. 2023. Conserved and divergent mechanisms of inner kinetochore assembly onto centromeric chromatin. *Current Opinion in Structural Biology* **81**:102638. DOI: https://doi.org/10.1016/j.sbi.2023.102638, PMID: 37343495

Zaret KS. 2020. Pioneer transcription factors initiating Gene Network changes. *Annual Review of Genetics* **54**:367–385. DOI: https://doi.org/10.1146/annurev-genet-030220-015007, PMID: 32886547

Zhong Y, Wang G. 2020. Three-Dimensional single particle tracking and its applications in confined environments. *Annual Review of Analytical Chemistry* **13**:381–403. DOI: https://doi.org/10.1146/annurev-anchem-091819-100409, PMID: 32097571

Zhou K, Gaullier G, Luger K. 2019. Nucleosome structure and dynamics are coming of age. *Nature Structural & Molecular Biology* **26**:3–13. DOI: https://doi.org/10.1038/s41594-018-0166-x, PMID: 30532059